

ACCURACY OF INTERPOLATED BATHYMETRIC DIGITAL ELEVATION MODELS

by

CHRISTOPHER JOSEPH AMANTE

B.A., College of the Holy Cross, 2009

A thesis submitted to the  
Faculty of the Graduate School of the  
University of Colorado in partial fulfillment  
of the requirement for the degree of  
Master of Arts  
Department of Geography

2012

This thesis entitled:  
Accuracy of Interpolated Bathymetric Digital Elevation Models  
written by Christopher Joseph Amante  
has been approved for the Department of Geography

---

Waleed Abdalati

---

Barbara Buttenfield

---

Barry Eakins

Date \_\_\_\_\_

The final copy of this thesis has been examined by the signatories, and we find that both the content and the form meet acceptable presentation standards of scholarly work in the above mentioned discipline.

Amante, Christopher J. (M.A., Geography)  
Accuracy of Interpolated Bathymetric Digital Elevation Models  
Thesis directed by Associate Professor Waleed Abdalati

Digital elevation models (DEMs) are the framework for the modeling of numerous coastal processes including tsunami propagation and inundation, storm-surge, and sea-level-rise. The National Oceanic and Atmospheric Administration (NOAA) National Geophysical Data Center (NGDC) develops integrated bathymetric-topographic DEMs across coastal zones to support tsunami propagation and inundation modeling efforts. The development of integrated bathymetric-topographic DEMs requires extreme interpolation across large distances between sparse bathymetric measurements in order for the model to retain the resolution of dense coastal topographic data, particularly lidar. This study examines the accuracy of three common interpolation methods used to develop bathymetric DEMs of Kachemak Bay, Alaska: inverse distance weighting (IDW), spline, and triangular irregular network (TIN). The goal of the study is to examine the relationship between interpolation deviations from measured depths and sample density, distance to the nearest depth measurement, and terrain characteristics.

A split-sample method was used to determine that the accuracy of the three evaluated interpolation methods decreases in areas of high surface curvature, at greater distances from the nearest measurement, and at smaller sampling densities. Furthermore, spline is the most accurate interpolation method at all sampling densities. Predictive equations of interpolation uncertainty derived from the quantification of interpolation deviations in relationship to sample density and distance to the nearest depth measurement were developed. These predictive equations of the uncertainty in DEMs introduced by interpolation methods can aid mitigation efforts for coastal communities prone to tsunamis, storm-surge, and other coastal hazards, by improving the understanding of the propagation of uncertainty into the modeling of such coastal processes that rely on integrated bathymetric-topographic DEMs.

## ACKNOWLEDGEMENTS

I am very thankful for the members of my committee who provided invaluable guidance throughout this project. Waleed Abdalati, who accepted me as his student, and was always there to offer academic advice despite being relocated to Washington, D.C. to become the Chief Scientist at NASA, and Barbara Battenfield, whose course in GIS modeling provided the technical background needed to accomplish many of the required tasks. Most of all, I am deeply appreciative of Barry Eakins, who changed the course of my life by selecting me for an undergraduate summer internship at NOAA in Boulder, which then became my first full-time job, and subsequently led to a graduate research assistantship through CIRES at NOAA. Barry's constant mentorship is largely responsible for my professional development, in addition to being the primary guiding force of this research.

I would also like to thank many others at NOAA NGDC, especially Lisa Taylor, Sue McLean, and Chris Fox, for their support, and the National Tsunami Hazard Mitigation Program and CIRES, which provided funding for this research. Lastly, I am grateful for my colleagues at NGDC, Kelly Carignan, Pamela Grothe, Dorothy Friday, Elliot Lim, and especially Mathew Love, for all of their help throughout this project.

## TABLE OF CONTENTS

LIST OF TABLES .....	vi
LIST OF FIGURES .....	vii
CHAPTER 1: INTRODUCTION .....	1
1.1 Bathymetric Digital Elevation Models .....	2
1.2 Depth Measurement Uncertainty .....	4
1.3 Interpolation Methods .....	6
CHAPTER 2: DATA & KACHEMAK BAY, ALASKA STUDY AREA .....	13
2.1 Hydrographic Survey .....	13
2.2 Measured Depth Raster .....	14
2.3 Semivariogram .....	15
2.4 Slope & Curvature .....	16
CHAPTER 3: METHODOLOGY .....	19
3.1 Split-sample Process .....	19
3.2 Raster Query .....	21
3.3 Data Buffers .....	23
3.4 Optimization of Interpolation Parameters .....	27
3.5 Correlations .....	28
3.6 Median Percent Deviation Maps.....	29
CHAPTER 4: RESULTS .....	32
4.1 Optimal Interpolation Parameters .....	32
4.2 Interpolation Deviations & Sampling Density .....	37
4.3 Correlations .....	40
4.4 Interpolation Deviations & Terrain .....	44
4.5 Median Percent Deviation Maps.....	46
4.6 Interpolation Deviations & Distance to the Nearest Measurement .....	55
4.7 Predictive Equations of Interpolation Uncertainty .....	60
CHAPTER 5: DISCUSSION & CONCLUSIONS .....	65
LITERATURE CITED .....	69

## LIST OF TABLES

Table 1. Evaluated Interpolation Method Parameters.....	27
Table 2. Median Distance to the Nearest Measurement Raster Statistics.....	30
Table 3. Optimal Interpolation Method Parameters .....	36
Table 4. Equations to Estimate Interpolation Uncertainty from the Sampling Density .....	39
Table 5. Relationship between Sampling Density and Median Distance to the Nearest Measurement.....	39
Table 6. Equations to Estimate Interpolation Uncertainty from the Distance to the Nearest Measurement for Various Sampling Densities .....	64

## LIST OF FIGURES

Figure 1. Perspective Image of an Integrated Bathymetric-topographic DEM .....	3
Figure 2. Example of Higher Depth Measurement Uncertainty .....	5
Figure 3. Location of Kachemak Bay, AK Study Area .....	13
Figure 4. Measured Depth Raster of Kachemak Bay .....	15
Figure 5. Semivariogram of Kachemak Bay Depths .....	16
Figure 6. Slope Raster of Kachemak Bay .....	17
Figure 7. Curvature Raster of Kachemak Bay .....	18
Figure 8. Split-sample Methodology for Quantifying Interpolation Deviations .....	21
Figure 9. Raster Query Methodology .....	23
Figure 10. Data Buffer .....	24
Figure 11. Histogram of the Distances to the Nearest Measurement .....	25
Figure 12. Region of Analysis .....	26
Figure 13. Histogram of the Median Distance to the Nearest Measurement Raster.....	30
Figure 14. Standard Deviation of all Evaluated Combinations of Parameters .....	33
Figure 15. Comparison of Spline Parameters .....	35
Figure 16. Absolute Median Percent Deviation and Sampling Density .....	37
Figure 17. Spearman’s Correlation Rho between Absolute Percent Deviation and Distance to the Nearest Measurement.....	40
Figure 18. Spearman’s Correlation Rho between Absolute Percent Deviation and Slope.....	41
Figure 19. Spearman’s Correlation Rho between Absolute Percent Deviation and Absolute Curvature.....	42
Figure 20. Spearman’s Correlation Rho between Percent Deviation and Curvature .....	43
Figure 21. Relationship between TIN Interpolation Deviations and Curvature .....	44
Figure 22. Absolute Median Percent Deviation and Slope.....	45
Figure 23. Median Percent Deviation and Curvature .....	46
Figure 24. IDW Median Percent Deviation .....	47
Figure 25. Spline Median Percent Deviation .....	47
Figure 26. TIN Median Percent Deviation .....	48
Figure 27. Inset of Measured Depths with Variable Slope and Curvature .....	49
Figure 28. Slope Inset .....	50
Figure 29. Curvature Inset .....	50
Figure 30. IDW Median Percent Deviation Inset .....	51
Figure 31. Spline Median Percent Deviation Inset .....	51
Figure 32. TIN Median Percent Deviation Inset.....	52
Figure 33. Median Percent Deviation Profiles.....	53
Figure 34. Curvature Profile .....	53
Figure 35. Slope Profile .....	54
Figure 36. Median Interpolated Depths Profiles.....	55
Figure 37. Inset of Measured Depths with Locations of Measurements used for Interpolation...	56
Figure 38. IDW Interpolated Surface.....	57
Figure 39. IDW Profile .....	58
Figure 40. Spline Profile.....	59
Figure 41. TIN Profile.....	59

Figure 42. Absolute Median Percent Deviation and Distance to the Nearest Measurement at a 1% Sampling Density.....	61
Figure 43. Absolute Median Percent Deviation and Distance to the Nearest Measurement at a 5% Sampling Density.....	61
Figure 44. Absolute Median Percent Deviation and Distance to the Nearest Measurement at a 10% Sampling Density .....	62
Figure 45. Absolute Median Percent Deviation and Distance to the Nearest Measurement at a 25% Sampling Density .....	62
Figure 46. Absolute Median Percent Deviation and Distance to the Nearest Measurement at a 50% Sampling Density .....	63

## CHAPTER 1: INTRODUCTION

The research completed for this master's thesis builds on previous studies that investigated the accuracy of spatial interpolation methods used to develop digital elevation models (DEMs). Interest in the accuracy of interpolation methods spans numerous academic disciplines including geography, hydrology, oceanography, geophysics, environmental science, and hazards. While almost all previous studies focus on the accuracy of interpolation methods in developing DEMs from dense topographic data, this research is unique in that it addresses the accuracy of interpolation methods used to develop bathymetric DEMs from sparse bathymetric data. The accuracy of an interpolation method refers to the closeness of interpolated values to accepted values. In this study, measured depths are considered the accepted values. Interpolation accuracy is inversely related to the magnitude of deviations from measured depths, and thus interpolation methods with smaller deviations from measured depths are considered more accurate. However, interpolation is typically used in areas without measured depths, and thus the interpolation accuracy cannot be quantified. The lack of knowledge about interpolation deviations from accepted values represents the uncertainty introduced into DEMs by interpolation methods.

There is currently a lack of literature on predictive equations of interpolation uncertainty. There is widespread use of DEMs developed with interpolation methods across numerous disciplines in the academic, government, and private sectors with little or no accompanying estimates of the uncertainty inherent in the models. The significance of estimating the uncertainty of DEMs ranges from academically and commercially beneficial to potentially life-saving. Estimating DEM uncertainty can aid academic research that utilize DEMs including

stream-flow, sediment-transport, and soil-landscape modeling, as well as commercial interests in natural resource extraction. Similarly, the modeling of hazards such as tsunami inundation and hurricane storm-surge inundation require integrated bathymetric-topographic DEMs (Eakins and Taylor, 2010) typically developed with interpolation methods. Flood maps and subsequent evacuation routes are derived from such modeling, and estimating and then communicating the uncertainty inherent in the models and flood maps to the public can potentially mitigate future human losses.

To address these issues, this thesis investigates the accuracy of three common spatial interpolation methods used to develop bathymetric DEMs: inverse distance weighting (IDW), spline, and triangular irregular network (TIN). The primary objective of this research is to assess the accuracy of these interpolation methods and the relationship between their deviations from measured depths and sampling density, distance to the nearest measurement, and terrain characteristics. After quantifying and characterizing the accuracy of various interpolation methods, predictive equations of interpolation uncertainty using distance to the nearest measurement and sampling density are presented. Such equations of interpolation uncertainty can provide valuable insight on the propagation of DEM uncertainty introduced by interpolation methods into the modeling of numerous oceanic, coastal, and land processes.

### *1.1 Bathymetric Digital Elevation Models*

The oceans are truly Earth's last great unknown. Surprisingly, the surfaces of Mars, Venus, and the Earth's moon are mapped at a higher-resolution than the seafloor (Smith, 2004), as individual soundings can have data gaps of hundreds of kilometers in the Earth's oceans (Smith and Sandwell, 1997). The National Oceanic and Atmospheric Administration (NOAA)

National Geophysical Data Center (NGDC) archives hydrographic surveys that date back to 1837 (<http://www.ngdc.noaa.gov/mgg/bathymetry/hydro.html>). These surveys provide depth measurements at discrete locations, and more recent digital surveys are commonly stored in vector format. However, a continuous representation of the seafloor is typically required for the modeling of numerous oceanic and coastal processes including ocean circulation, tsunami propagation, and hurricane storm-surge. Bathymetric DEMs are continuous representations of the seafloor that are derived from depth measurements and are commonly stored in raster format comprised of a matrix of rectangular cells with each cell representing the average depth of the area contained within the cell (Figure 1).

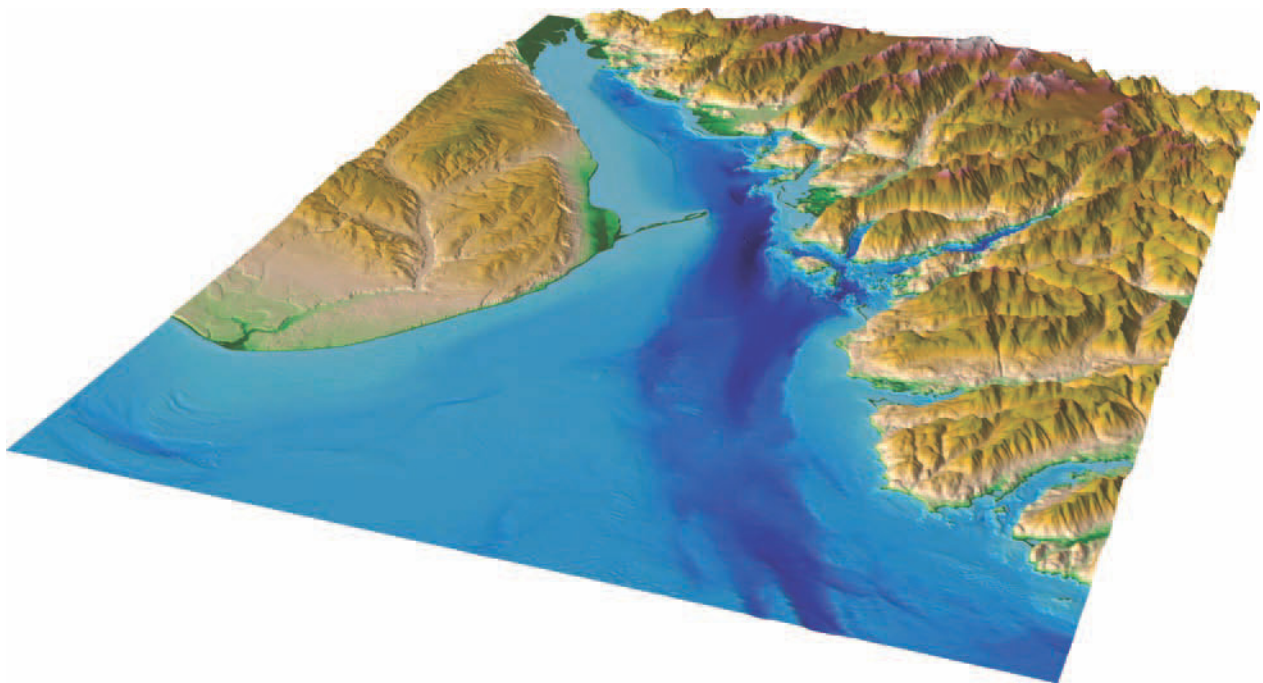


**Figure 1. Perspective image of an integrated bathymetric-topographic DEM of Kachemak Bay, Alaska in raster format with 2-times vertical exaggeration (Friday et al., 2010). Dark blue coloring denotes areas of deeper bathymetry, while dark orange and red coloring denotes areas of higher topography.**

NOAA NGDC develops integrated bathymetric-topographic DEMs across coastal zones to support tsunami propagation and inundation modeling efforts. The development of integrated

bathymetric-topographic DEMs requires extreme interpolation across large distances between sparse bathymetric measurements in order for the model to retain the resolution of the dense coastal topographic data, particularly lidar. The accuracy of such extreme interpolation is unknown, and therefore an unknown degree of uncertainty is propagated into tsunami propagation and inundation models.

### *1.2 Depth Measurement Uncertainty*

Integrated bathymetric-topographic DEMs are the framework for the modeling of numerous oceanic and coastal processes including ocean circulation, tsunami propagation, and tsunami inundation (Eakins and Taylor, 2010). For example, the direction and magnitude of the energy of tsunami wave propagation and inundation is significantly impacted by both deep-ocean bathymetry (Kowalik et al., 2008) and coastal bathymetry (Horillo et al., 2008). The speed of the wave is determined by the depth, and the deeper the water, the faster the wave travels (Satake, 1988). Consequently, as the tsunami travels over ridges, seamounts, and submarine canyons with various depths, segments of the wave travel at different speeds, causing the energy to change direction due to refraction. The accuracy of modeling oceanic and coastal processes such as tsunami propagation and inundation is therefore partly dependent on the accuracy of the DEM, which is primarily determined by the quality of the depth measurements. As a result, uncertainty in the depth measurements propagates into uncertainty in the modeling of such processes.

Uncertainty in the depth measurements can originate from the platform, instrumentation, environment, integration, or calibration, and take the form of horizontal or vertical uncertainty or both (Figure 2; Hare et al., 2011). These sources of uncertainty are easier to quantify than other non-probabilistic sources of measurement uncertainty. For example, there is uncertainty in what

object is actually being detected by sonar or lidar measurements, such as suspended sediments, or penetration into the seafloor as a result of the sonar/lidar frequency and impedance of the material of the seabed (Hare et al., 2011). Other non-probabilistic forms of measurement uncertainty are even more difficult to quantify, such as the temporal change of the seafloor.

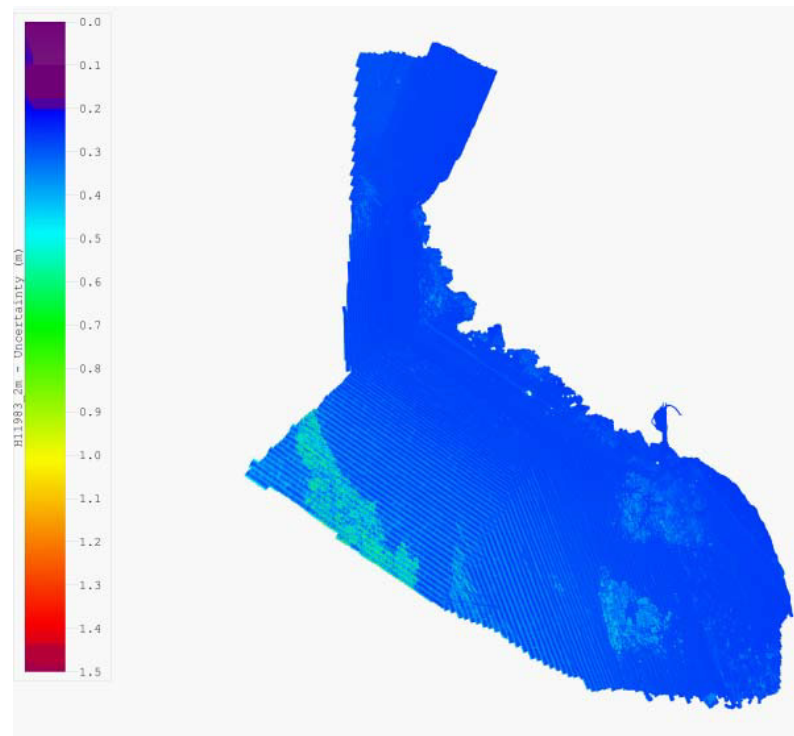


**Figure 2. An example of higher depth measurement uncertainty indicated by green coloring due to sound velocity errors (stripes), and to rougher seafloor topography in the lower left portion of the figure (U.S Department of Commerce - NOAA, 2008; NOS Survey H11983).**

While the accuracy of DEMs is primarily determined by the quality of the depth measurements, the low spatial resolution of especially older bathymetric soundings necessitates the use of interpolation methods to estimate areas of unknown depths. Consequently, the accuracy of modeling coastal processes is also partly dependent on the accuracy of the interpolation method used to develop the continuous representation of the seafloor.

### 1.3 *Interpolation Methods*

Interpolation is a mathematical process of predicting the values of unknown locations based on surrounding measured values (Burrough and McDonnell, 1998). Interpolation requires two basic assumptions about the surface, that the surface is continuous and smooth, and that the neighboring data points have high correlation with the unknown area (Liu, 2007). Several different interpolation techniques exist for creating surfaces, including IDW, spline, TIN, natural neighbor, and kriging, all of which can create different DEM surfaces, even when built from the same source data (Maune et al., 2007).

There are numerous interpolation methods, but all are based on the same assumption that bathymetry is spatially autocorrelated. The notion of spatial autocorrelation is largely attributed to Tobler's 1<sup>st</sup> law of geography, "Everything is related to everything else, but near things are more related than distant things (Tobler, 1970)." That is, the depth at one location is more similar to depths nearby than the depths far away. The different mathematical algorithms used in each interpolation method produce divergent DEMs, even when developed from the same source data.

Interpolation methods can be classified into general groups based on the assumptions and features used to estimate the depths of unknown areas using known measurements. Interpolation methods can be classified as either geostatistical or deterministic, local or global, and exact or inexact (Li and Heap, 2008). Geostatistical methods, such as kriging, use both mathematical and statistical functions to estimate depths, while deterministic methods, such as spline, IDW and TIN, use the measurements directly and mathematical functions only to predict unknown values (Childs, 2004). Geostatistical methods are typically more computationally and time-intensive in order to accurately quantify the statistical relationship between depths compared to deterministic methods, which have simpler parameters and are computationally faster (Bloschl and Grayson,

2001; Castiglioni et al., 2009). Local methods use a subset of measurements surrounding the location to be predicted and global methods use all available measurements (Burrough and McDonnell, 1998). Local methods are preferred when the seafloor structure is driven by local variation, and global methods should be used when the seafloor structure is driven by a trend over a larger area.

Lastly, exact interpolators always honor the measurements by creating a surface that have the same values at the locations of measurements, in contrast to inexact interpolators, which are not constrained by the depth measurement values at those locations (Burrough and McDonnell, 1998). Inexact interpolators can add additional uncertainty to the model by creating surfaces that diverge from the measurements (Hare et al., 2010), but can be useful when there is already large measurement uncertainty. Interpolation methods can be any combination of geostatistical or deterministic, local or global, and exact or inexact, and the method should be chosen based on the data quality, sampling distribution, terrain characteristics, and computational resources. More specifically, each interpolation method has particular mathematical constraints for predicting unknown values.

Three deterministic methods were analyzed in this study because unlike geostatistical methods, deterministic methods do not provide an assessment of uncertainty along with the predicted values (Li and Heap, 2008). The first method, IDW, is a deterministic, local, exact interpolator that predicts values using a linearly-weighted combination of sample points (Liu, 2007). The weight is a function of inverse distance and is raised to a user-defined mathematical power that controls the significance of known measurements based on their distance from the location to be predicted. A higher power results in distant measurements having less influence, which produces a more detailed and less smooth surface. Conversely, a lower power results in

distant measurements having a greater influence and results in smoother surfaces. The number of measurements used for prediction can also be defined, with more depths resulting in smoother surfaces and more similar to global interpolation.

The main strength of IDW is its simplicity, which makes it easy to use and computationally fast. Akkala et al. (2010) also found IDW to work well with noisy data. Since IDW uses a weighted-average algorithm, the interpolated surface smoothes measurement errors. However, the weighted-average aspect is also one of the many disadvantages of IDW, as predicted values will always fall within the range of values of the input data and thus peaks and valleys cannot be predicted unless they have been sampled (Declercq, 1996). Another disadvantage is that the spatial arrangement of samples does not affect the weighting scheme (Myers, 1994; Akkala et al., 2010). The weight of samples is only determined by the user-defined power and the distance from the measurement, and therefore the algorithm cannot take in consideration the degree of spatial correlation. Also, the user-defined size of the search window and power affects the quality of the interpolated surface (Isaaks and Srivastava, 1989; Burrough and McDonnell, 1998; Akkala et al., 2010). The most typical artifact created by IDW interpolation is the “bulls-eye” effect created at the location of sample points (Erdogan, 2009). Akkala et al. (2010) found that the best-suited scenario is moderately dense sampling with regard to local variation.

The second method evaluated was spline interpolation. There are numerous types of spline interpolation, including thin plate spline, regularized spline, and spline with tension. Thin plate spline produces a locally smoothed average that is an inexact interpolator (Burrough and McDonnell, 1998), while spline with tension and regularized spline are exact interpolators (Mitas and Mitasova, 1988). The two exact interpolators, regularized spline, and spline with tension,

were evaluated in this study. In addition to being exact, these two spline types are deterministic and local interpolation methods. The regularized method creates a smooth, gradually changing surface and allows for values above and below the measurement values (ESRI, 2010). The tension method creates a less smooth surface and is more closely constrained by the sample data range (ESRI, 2010). A user can further fine-tune spline interpolation by the number of points and a weight parameter. The greater the number of points specified, the greater the influence of distant points and the smoother the surface. For regularized spline, a greater weight results in a smoother surface (ESRI, 2010). On the contrary, a greater weight results in a coarser surface for spline with tension (ESRI, 2010).

There are many advantages and disadvantages to spline interpolation. In contrast to trend surfaces and weighted-averages, spline interpolation retains local features (Burrough and McDonnell, 1998). In addition, spline can predict values outside of the data range, interpolating peaks and valleys if they were not sampled (Childs, 2004). Also, spline interpolation creates visually appealing curves or contour lines (Akkala et al., 2010). This method is best used for gently varying terrain as it can introduce “overshoots” in areas of large gradients (Mitas and Mitasova, 1999). While spline interpolation can predict maximum and minimum values greater than and less than the values of the sampled data, this allows for the previously mentioned “overshoots” that create peaks and valleys where they don’t actually exist. Furthermore, spline interpolation can provide a view of reality that is unrealistically smooth (Burrough and McDonnell, 1998). Lastly, spline interpolation may mask measurement uncertainty in the data (Akkala et al., 2010). Akkala et al. (2010) found that the best-suited scenario for spline interpolation is irregularly-spaced data.

The third method evaluated is a vector representation of terrain, triangular irregular network (TIN). TINs are constructed by forming triangles between depth measurements using the Delaunay triangulation method. This method ensures that no measurements lie within the interior of any of the circumcircles of the triangles in the network, which maximizes the minimum interior angle of all triangles to avoid long, thin triangles (Soucy and Laurendeau, 1996).

The main advantage of TINs is the ability to represent the surface at different levels of resolution, which limits data redundancy in areas of uniform terrain while maintaining high resolution in areas of complex relief (Burrough and McDonnell, 1998; Akkala et al., 2010). TINs can also incorporate other features, such as streams and ridgelines, into the model if available in a polyline format. However, in most cases, TINs require visual inspection and manual control of the network (Akkala et al., 2010). Also, TINs are similar to weighted-average methods like IDW in that the minimum and maximum surface depths will be the same as the input depths and therefore peaks and valley will not be represented in the TIN surface unless they were sampled. Akkala et al. (2010) found that they best suited scenario for TINs was dense and moderate distribution of data points.

There is no single “best” interpolation method (Chaplot et al., 2006; Fisher and Tate, 2006), and the accuracy of all interpolation methods is degraded by heterogeneous seafloor morphology (Mackaness and Beard, 1993). The accuracy of all interpolation methods is related to the sampling density and distribution (MacEachren and Davidson, 1987; Aguilar et al., 2005; Anderson et al., 2005; Chaplot et al., 2006; Guo et al., 2010) and the terrain characteristics (Aguilar et al., 2005; Carlisle, 2005; Erdogan, 2009; Erdogan, 2010; Guo et al., 2010). Differences are largest in morphologically complex areas, areas of high curvature, where the

accuracy of all interpolation methods decreases. However, some interpolation methods more accurately represent different morphologic regimes.

Since depth is a spatially autocorrelated process, it is expected that interpolation deviations from the measured surface would also be spatially autocorrelated, with deviations greater in magnitude in areas of high curvature. Furthermore, since interpolation deviations are a non-stationary process, a global statistic, such as root mean square error (RMSE) or mean absolute error (MAE), is often insufficient in characterizing the accuracy of the interpolation method (Carlisle, 2005). In areas of flat terrain, the interpolation deviations are presumably very small, whereas the interpolation deviations are larger in areas of high curvature. The inadequacy of global measures of accuracy has been addressed by creating deviation maps that spatially visualize clusters of high and low accuracy (Carlisle, 2005; Erdogan, 2009).

The overarching goal of this research is to characterize the relationship between interpolation accuracy and sampling density, distance to the nearest measurement, and terrain characteristics using sparse bathymetric data. While there is a clear relationship between sampling density and distance to the nearest measurement, a distinction is made as the random nature of the sampling density implemented in this study was capable of producing a wide-range of distances to the nearest measurement, especially at low sampling densities. Characterizing the accuracy of each method using various sampling densities and in different terrains will provide insight on the strengths and limitations of each method, and permit the derivation of equations that can be used to estimate DEM uncertainty introduced by interpolation.

Studies on divergent DEMs developed from different interpolation methods with dense topographic data have improved the understanding of the uncertainty of hydrologic modeling of stream flows (Peralvo and Maidment, 2004; Vazquez and Feyen, 2007). However, the

uncertainty of bathymetric DEMs developed from different interpolation methods with sparse depth measurements has yet to be comprehensively characterized and quantified. This research seeks to determine the interpolation method that most closely replicates measured bathymetry, using Kachemak Bay, Alaska as a representative region, by quantifying the interpolation deviations from the measured depths for each method for various sampling densities. In addition, this research will identify the optimal interpolation method parameters, quantitatively and qualitatively assess the relationship between interpolation deviations and terrain characteristics, and derive predictive equations of interpolation uncertainty based on the distance to the nearest measurement and sampling density.

## CHAPTER 2: DATA & KACHEMAK BAY, ALASKA STUDY AREA

### 2.1 Hydrographic Survey

The bathymetry of Kachemak Bay, Alaska (Figure 3) was used to quantify the interpolation deviations from measured depths and assess the relationship between interpolation deviations and sampling density, distance to the nearest measurement, and terrain characteristics. Kachemak Bay was chosen because of its varying terrain that ranges from areas of constant depths to areas of rapidly changing depths. An area with varied terrain was chosen in order to evaluate the effect of terrain on interpolation deviations, with the initial assumption that interpolation deviations would be greatest in magnitude in areas of high surface curvature. Kachemak Bay is fed by glacial run-off and the area surveyed has a variety of glacial sediments covered by a layer of sand that produces several types of bedforms and changes in depths (Bouma et al., 1980).

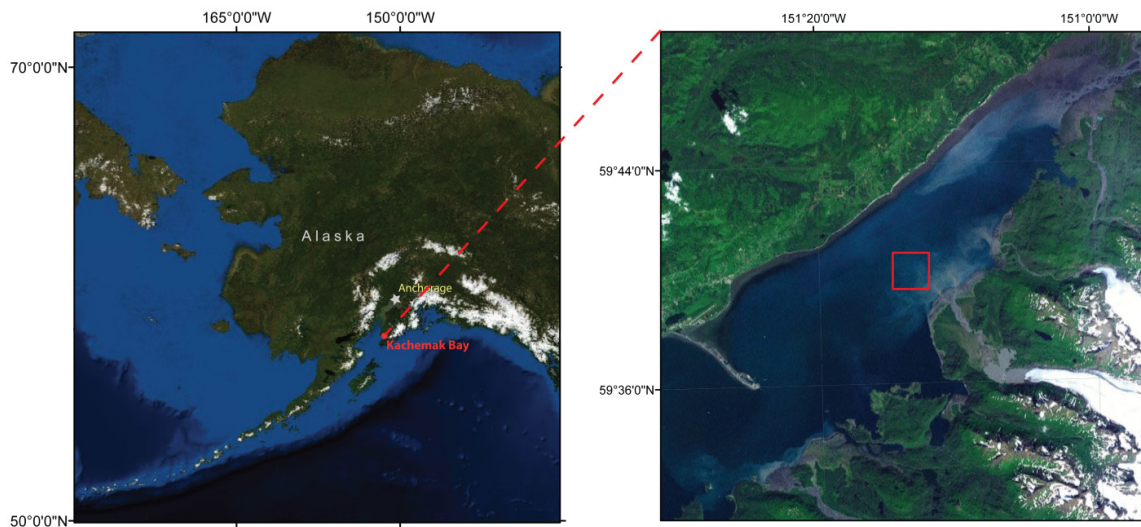


**Figure 3. Location of Kachemak Bay, AK study area; red box outlines area of analysis. Background is ESRI World 2D imagery (ESRI, 2009).**

Kachemak Bay was surveyed in 2008 with high-resolution multibeam swath sonar as part of a large-scale project called NOAA Hydropalooza (<http://www.hydropalooza.noaa.gov/>). The goal of the project was to map Kachemak Bay's seafloor and coastline to support safe maritime transportation, protect coastal communities, assess fisheries and critical marine habitats, and to better understand the Bay. The digital hydrographic survey, H11934, was downloaded from the NGDC National Ocean Service (NOS) Hydrographic Survey database (<http://www.ngdc.noaa.gov/mgg/bathymetry/hydro.html>) in Bathymetric Attributed Grid (BAG) format. The survey was downloaded as a thoroughly evaluated combined BAG with a 4-meter horizontal resolution referenced to UTM Zone 5 North.

## 2.2 *Measured Depth Raster*

The survey BAG was converted to XYZ (eastings, northings, depth) format, then averaged using the Environmental Systems Research Institute (ESRI) ArcGIS 10.0 (<http://www.esri.com/>) 'Point to Raster' tool at a 10-meter by 10-meter cell size. This averaging ensured that every 10-meter cell had one constraining data point derived from depth measurements (Figure 4).

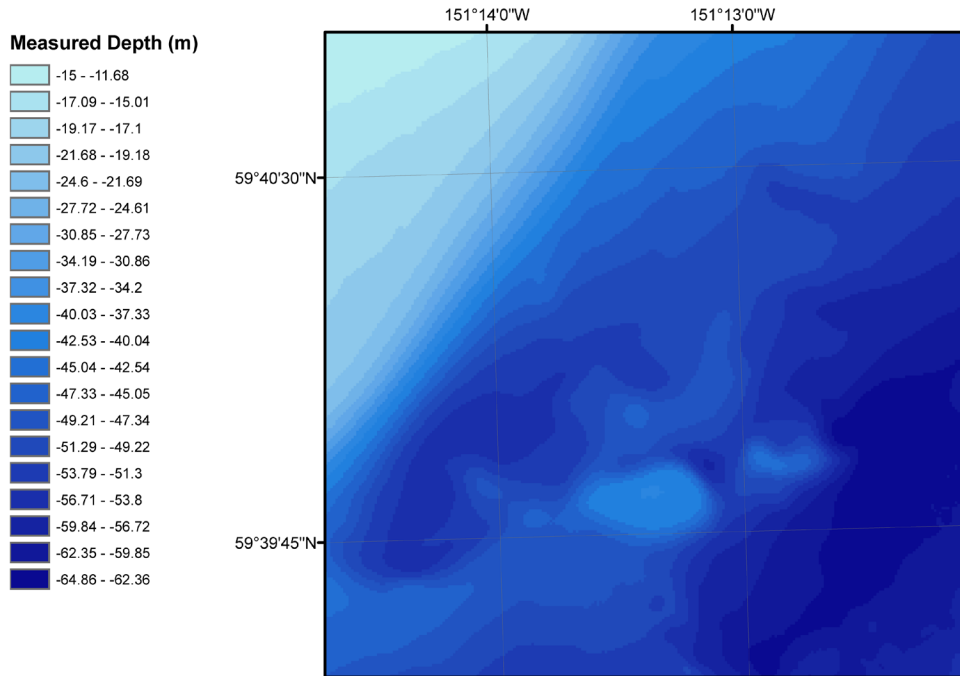


**Figure 4. Measured depth raster of Kachemak Bay with no interpolation at a 10-meter cell size.**

### 2.3 *Semivariogram*

The degree of spatial autocorrelation of the measured Kachemak Bay depth raster was quantified using a semivariogram. Spatial autocorrelation is the statistical correlation between an attribute (e.g., depth) and distance, with the assumption that the values of an attribute nearby are typically more similar than the values farther apart (Tobler, 1970). The semivariogram shows the variance or the difference between every depth measurement paired with another measurement in the study area as a function of the distance between the depths. The distance at which the variance levels off is known as the range, which defines the distance at which depths are no longer spatially autocorrelated. Quantifying the spatial autocorrelation can aid in the selection of interpolation parameters, particularly the search radius for IDW. The semivariogram below was developed using a random 1% sampling of the measured depths as the focus of this study was on interpolation across large distances. The model of the semivariogram indicates that depths

separated by a distance greater than approximately 200 meters (20 cells) have little or no spatial autocorrelation and are not useful for interpolation (Figure 5).

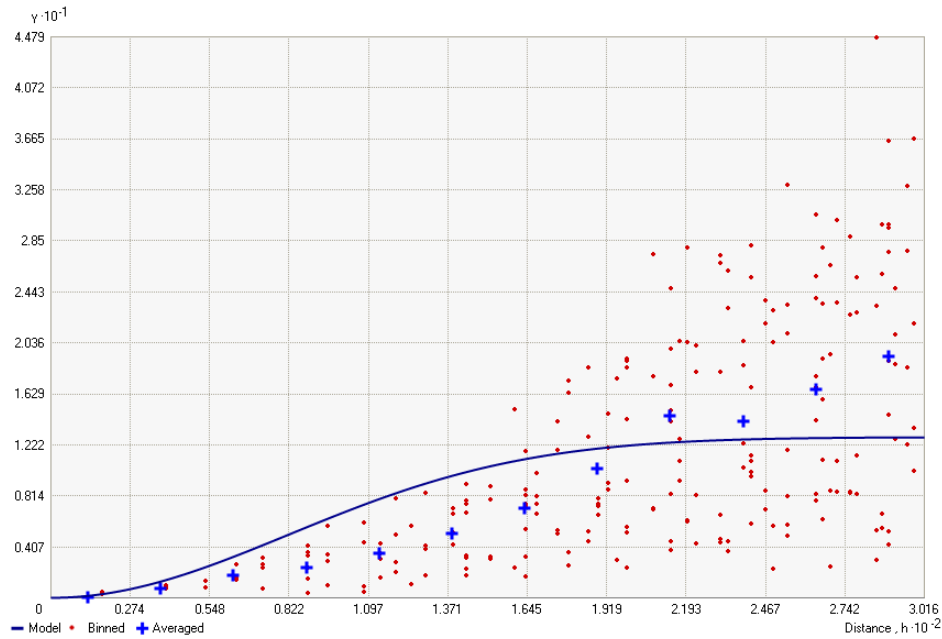


**Figure 5. The semivariogram of a random 1% sampling of depths of Kachemak Bay.**

#### 2.4 *Slope & Curvature*

Slope and curvature rasters were derived from the original measured depth raster with no interpolation using ArcGIS 10.0. The slope (also referred to as gradient) represents the maximum rate of change of depths in a 3 by 3 cell window that is moved over the entire original depth raster (Figure 6; Burrough and McDonnell, 1998). A greater slope (units in degrees) corresponds to steeper surfaces.

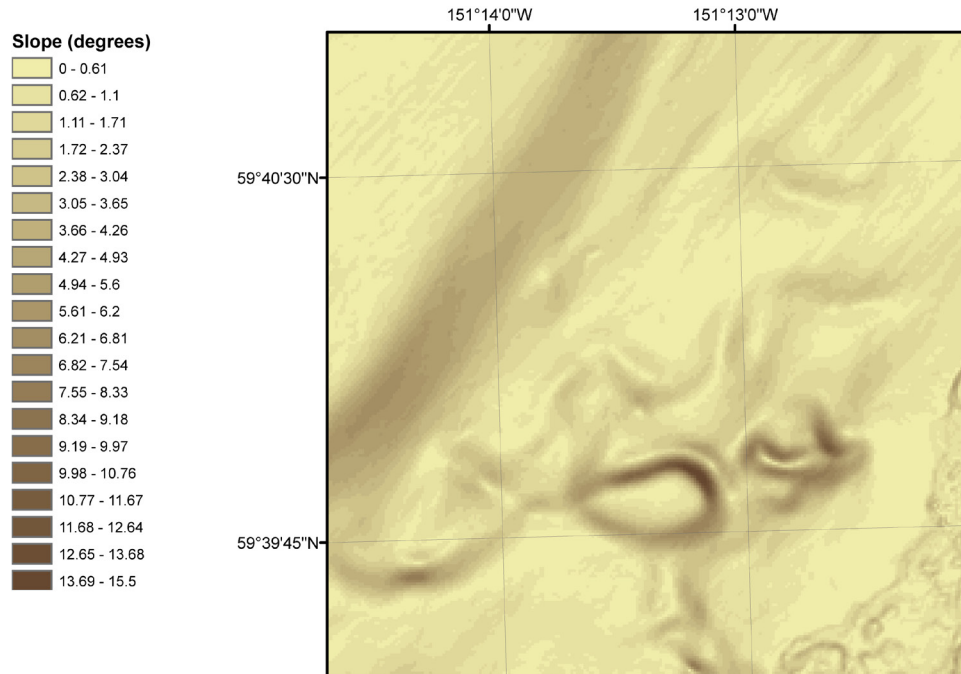


**Figure 6. Slope of the Kachemak Bay study area derived from the measured depth raster.**

Curvature is the rate of change of the slope, or the slope of the slope. There are three types of curvature: profile, plan, and total curvature. Profile and plan curvatures are the curvatures on a line formed by the intersection of a plane and the terrain surface. The curvature of a line is the reciprocal of the radius of curvature, so a gradually changing curve has a small curvature, while a tight curve has a large curvature (Galant and Wilson, 2000). Profile curvature represents the rate of change of slope in the direction of the maximum slope, which affects the acceleration and deceleration of flow and therefore influences erosion and deposition. Profile curvature also differentiates between upper and lower slopes (Galant and Wilson, 2000). The plan curvature represents the rate of change of the slope perpendicular to the direction of the maximum slope and influence convergence and divergence of flow and differentiates between ridges, valleys, and hillslopes (Galant and Wilson, 2000). The total curvature represents the curvature of the surface itself, not the curvature of a line across the surface in a given direction

(Galant and Wilson, 2000). A positive total curvature value represents an upwardly convex surface, while a negative total curvature value represents an upwardly concave surface. A zero curvature value represents an area of constant slope (Figure 7). In addition to the slope, the total curvature was used to characterize the relationship between interpolation deviations and terrain characteristics.

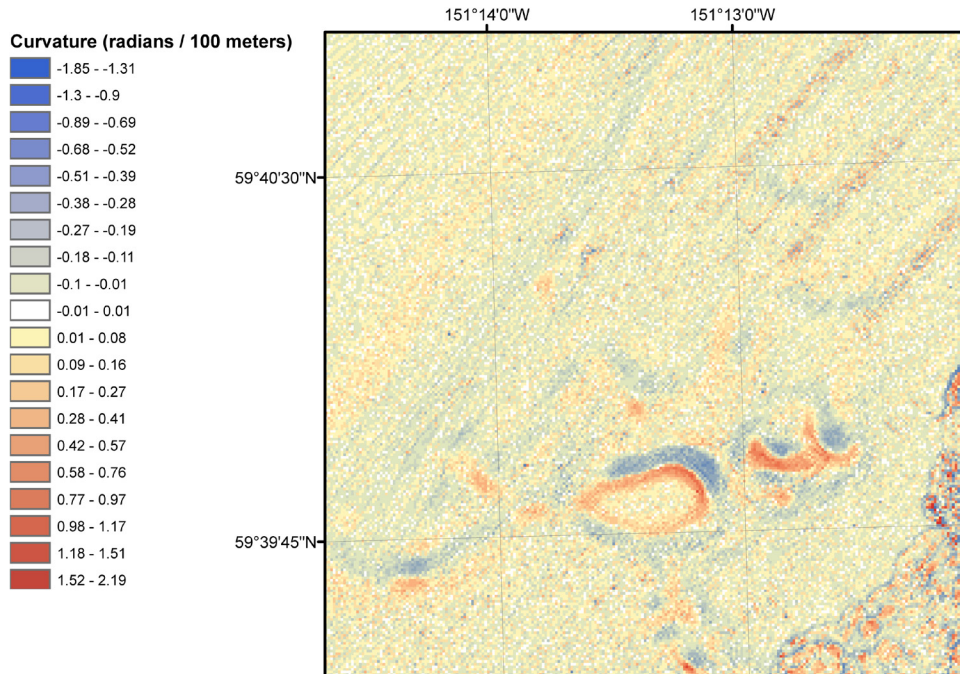


**Figure 7. Curvature of the Kachemak Bay study area derived from the measured depth raster.**

## CHAPTER 3: METHODOLOGY

The accuracy of the three deterministic interpolation methods was analyzed in this study using ArcGIS 10.0. Desmet (1997) defines the accuracy of interpolation methods used to develop DEMs as a compromise between “precision” and “shape reliability”. Precision can be evaluated by comparing interpolated depths to measured values using non-spatial, dimensionless indices such as MAE or RMSE, while shape reliability is evaluated through statistical analysis of the spatial properties of a surface, such as slope and curvature (Desmet, 1997; Chaplot et al., 2006). In this study, the accuracy of interpolation methods refers to the precision described by Desmet (1997) and the “shape reliability” of the individual methods was not investigated. Although Declercq (1996) found that accurate interpolation methods do not necessarily preserve spatial patterns, a comprehensive evaluation of the “shape reliability” of the interpolation methods was outside of the scope of this research. Furthermore, the original measured depths are considered “true” depths and the uncertainties inherent in the measurements, as discussed in the first chapter of this thesis and by Hare et al. (2011) are ignored.

### *3.1 Split-sample Process*

There are numerous methods to assess the accuracy of interpolation methods. One approach is using a higher-resolution independent dataset to evaluate the accuracy of the interpolated surface (Chang and Tsai, 1991; Robinson and Metternicht, 2005; Fisher and Tate, 2006; Erdogan 2009). This is often not possible due to the time and monetary resources needed to collect the independent dataset. Furthermore, it would make little sense to develop a DEM using interpolation and sparse measurements if there was a higher-resolution DEM already

available. More often, cross-validation and split-sample methodologies are used to determine the accuracy of interpolation methods. Both cross-validation and split-sample use similar approaches. The most common form of cross-validation is the “leave one technique (Erdogan 2009).” This method consists of omitting one depth measurement prior to using an interpolation method, and then the difference between the interpolated depth and the omitted measured depth is calculated. This process is the repeated so that all depth measurements are omitted once. The differences between interpolated depths and omitted depths are then aggregated and an indication of the accuracy of the interpolation method is provided by a global statistics such as MAE or RMSE. A split-sample procedure uses exactly the same method as cross-validation except for one key difference. A split-sample procedure randomly omits a *percentage* of depth measurements (more than one depth measurement) at a time and calculates the differences between the omitted depths and interpolated depths. The split-sample method is often used to assess the stability of an interpolation method when using fewer measurements (Declerq, 1996; Smith et al., 2005; Erdogan, 2009).

A cross-validation procedure results in interpolating only 1 cell with depth measurements on all adjacent cells and may be more appropriate for interpolating dense data such as lidar. However, sparse hydrographic sounds collected using older single-beam sonar technology often necessitates extreme interpolation across many cells. This extreme interpolation between sparse bathymetric soundings is typically required for integrated topographic-bathymetric DEMs used for tsunami propagation and inundation modeling in order to retain the morphological detail of dense coastal, topographic lidar surveys (Hare et al., 2011). A split-sample method (Figure 8) was developed in this research to simulate a sparse bathymetric data set because of the interest in interpolating across many cells. The Kachemak Bay measured depth raster was the source for all

the random split-sample data sets. The split-sample process was repeated at the sampling densities to be used for analysis (1%, 5%, 10%, 25%, and 50%).

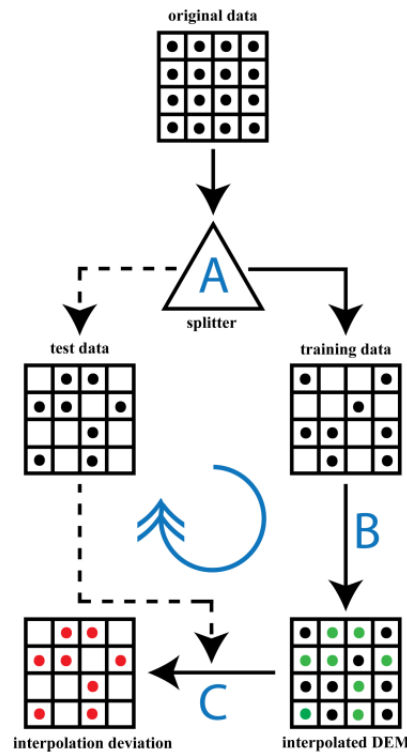


**Figure 8. Flowchart depicting the split-sample methodology for quantifying interpolation deviations.**

**A) The original data are averaged to have exactly one depth value per grid cell. They are then randomly split by a fixed percentage (e.g., 50%) into training and test data.**

**B) An interpolation method (e.g., spline) is applied to the training data to build an interpolated DEM.**

**C) The interpolated DEM is compared to the test data to quantify the interpolation deviations.**

**Steps A to C are repeated at the same split percentage (randomness resulting in different training and test data) to account for bathymetric variability. The method is run iteratively using different split-percentages to evaluate the stability (e.g., ability to reproduce the principal bathymetry) of the chosen interpolation method with various sampling densities.**

### 3.2 Raster Query

The deviations between the interpolated depths and the original measured depths were divided by the original measured depths and multiplied by 100 to obtain the interpolation percent deviation. The percent deviation was used in order to eliminate the effect of ocean depths on the

magnitude of deviations. For example, a 5 meter interpolation deviation in 10 meters of water is a more significant deviation than a 5 meter interpolation deviation in 1,000 meters of water, and is reflected by a 50% deviation compared to a 0.5% deviation, respectively. In addition, tsunami modeling requires more accurate, higher-resolution DEMs in shallow waters near-shore compared to less accurate, lower-resolution DEMs in deeper waters off-shore (Titov et al., 2003). Normalizing the deviation by the measured depth balances the importance of the absolute deviation for both shallow and deep waters. Furthermore, developing predictive equations of percent deviation will allow it to be used in any area of sparse measurements, from deep-ocean to shallow coastal waters.

After implementing the split-sample method, the Euclidean distance to the nearest measurement was calculated for every cell using the ArcGIS 10.0 'Euclidean Distance' tool. The distance was originally in map units (meters), but was transformed to raster cell units by dividing by the cell size (10-meters). The percent deviation was then compared on a cell-to-cell basis to the values of the distance to the nearest measurement raster, as well as the slope and curvature rasters derived from the original depths (Figure 9). The comparison between the rasters was then used to identify any relationships between the variables and to develop predicate equations of interpolation uncertainty that could be used in other areas of sparse depth measurements.

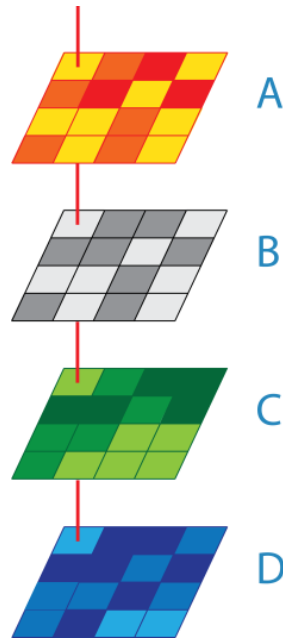


**Figure 9.** The interpolation percent deviations (A) are compared to the distance to the nearest measurement (B), slope (C), and curvature (D) rasters on a cell-to-cell basis in order to identify the relationship between percent deviations and these explanatory variables.

### 3.3 *Data Buffers*

To ensure an accurate analysis of the relationship between interpolation deviations and distance to the nearest measurement, and terrain characteristics, two data buffers were implemented to avoid edge effects. The first data buffer that was used to extract the depths along the borders in order to guide interpolation to the edge of the study area is shown in Figure 10.

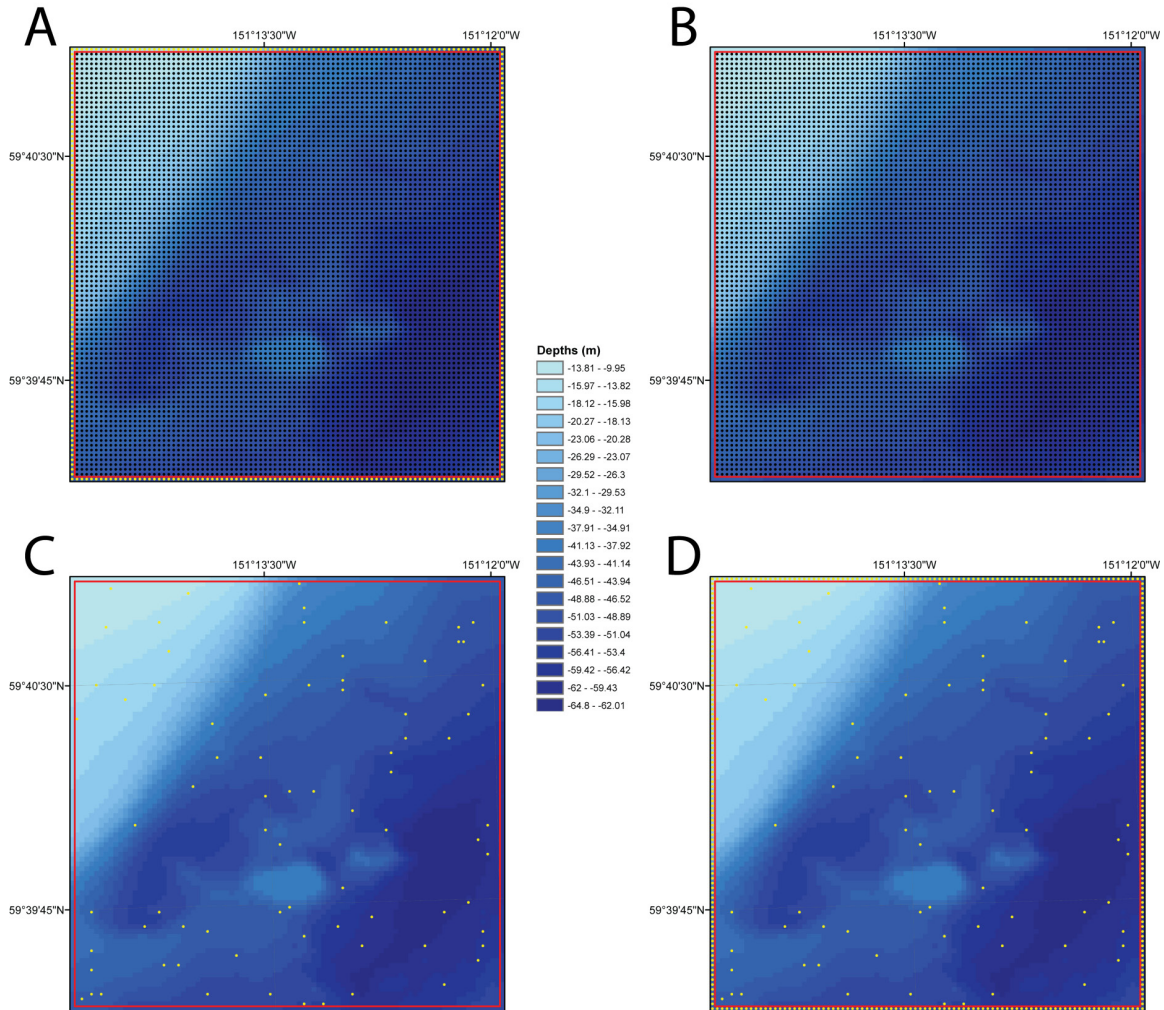


**Figure 10. Implementation of a data buffer to eliminate interpolation edge effects (shown at 30-meter cell size for visualization purposes).**

- A. The original measured depths are extracted from the perimeter of the study area (yellow points).**
- B. The border depths are removed, leaving only depths inside of the buffer (black points).**
- C. Depths are randomly selected at a given sampling density to be used for interpolation (e.g. 1%; yellow points).**
- D. The randomly selected points are merged with the border points to guide interpolation along the edges of the study area.**

There was a negative effect of the first data buffer that was implemented to always use depths along the border of the study area for interpolation. This data buffer resulted in cells adjacent to the inside of the border cells always being one cell away from a depth measurement.

Cells 2 away from the border were always less than or equal to 2 cells away from depth measurements, and so forth. A main research objective was to identify the relationship between interpolation deviations and distance to the nearest depth measurement. Since the cells near the border were always no less than a set distance away from a measurement, it would not have been possible to accurately identify the relationship between interpolation deviations and distance to the nearest measurement in these areas.

To determine how many cells should be excluded from analysis due to the bias of the border measurements, the split-sample process and subsequent “Euclidean Distance” tool was implemented using the lowest sampling density analyzed (1%), which would result in the greatest possible distances to the nearest depth measurement. The distances to the nearest measurement were aggregated, and it was found that 99% of the distances were less than 12 cells away from a measurement (Figure 11).

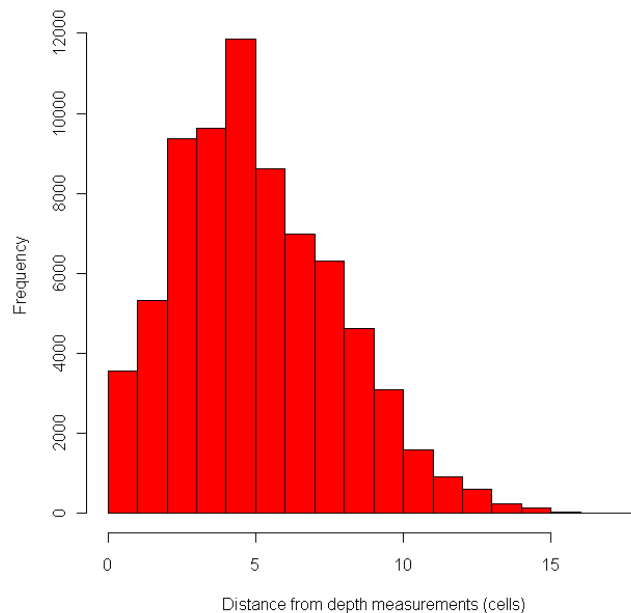


**Figure 11. Histogram of distances to the nearest depth measurement; 99% of cells are less than 12 cells away from a measurement when using a 1% sampling density.**

Thus, the area of analysis was restricted to a subset of the original study area by 12 cells on each side (Figure 12). This ensured that the edge of the area of analysis had a range of distances to the nearest measurement, without being biased towards the depths always kept along the outermost border of the study area. This subset for analysis also ensured that slope and curvature values were accurate by having a full 3 by 3 window for calculation.

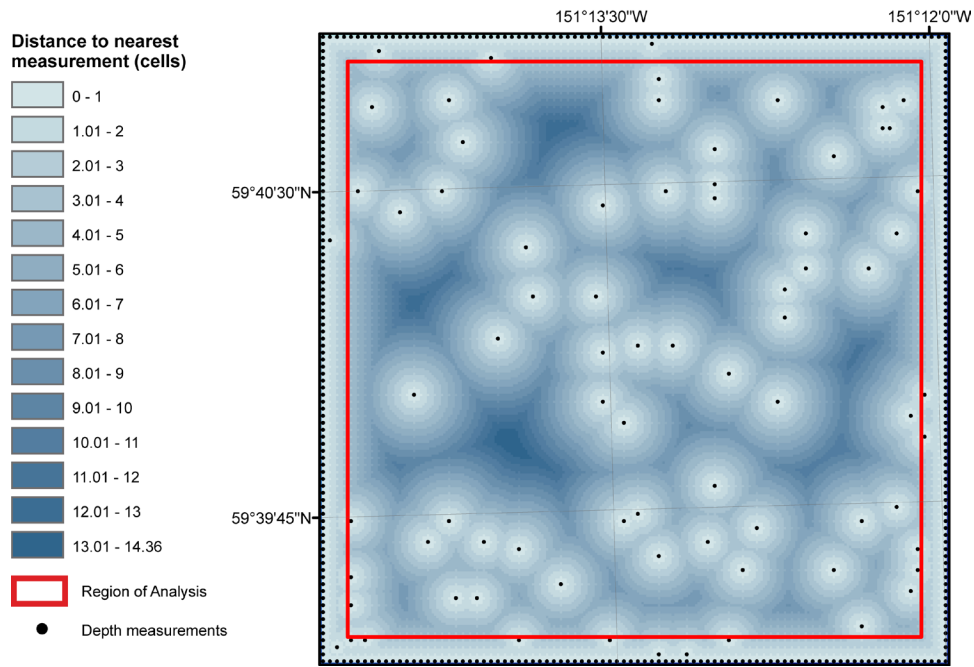


**Figure 12. An example of the distance to the nearest depth measurement raster created using the “Euclidean Distance” tool. The red box outlines the region of analysis (shown at 30-meter cell size for visualization purposes).**

The split-sample and raster query process was then repeated 200 times for all three methods with each method using exactly the same depth measurements for interpolation and evaluation to quantify the deviations. Each interpolation method always using the same depth measurements ensured an accurate comparison between the methods. The rationale for repeating the split-sample process 200 times is described in *Section 3.6*. The distance to the nearest

measurement, slope, and curvature values at the location of each deviation was queried and this process was repeated using 5 different sampling densities (1%, 5%, 10%, 25%, and 50%).

### 3.4 Optimization of Interpolation Parameters

Prior to assessing the accuracy of interpolation methods, the parameters of each method were optimized also using the same split-sample methodology. Using inappropriate parameters can cause significant artifacts in the interpolated surface, especially with IDW (Burrough and McDonnell, 1998; Akkala et al. 2010) and spline interpolation (Mitasova and Mitas, 1993; Cebecauer et al. 2002). Numerous parameters were evaluated with a brute-force methodology. Each interpolation method used all possible combinations of parameters evaluated, and the median percent deviation was calculated for every combination as an indicator of accuracy. Fifty combinations of IDW parameters, 60 combinations of spline parameters, and 2 TIN conversion to raster methods were evaluated (Table 1).

**Table 1. Interpolation method parameters evaluated for each method.**

<b>IDW Power</b>	<b>IDW Radius</b>	<b>Spline Type</b>	<b>Spline Number of Points</b>	<b>Spline Weight</b>	<b>TIN to raster conversion method</b>
1	Variable 4 points	Tension	20	0	Bilinear
2	Variable 8 points	Regularized	40	0.1	Natural Neighbors
3	Variable 12 points		60	0.5	
4	Variable 16 points		80	1	
5	Variable 20 points		100	5	
	Fixed 20 meters			10	
	Fixed 40 meters				
	Fixed 60 meters				
	Fixed 80 meters				
	Fixed 100 meters				

At each sampling percentage (1%, 5%, 10%, 25%, and 50%), the split-sample process was repeated three times using every combination of parameters to use different measurements for interpolation and account for bathymetric variability, and to ensure the identification of reasonable parameters. The combination of parameters that resulted in the smallest median percent deviation for each of the three interpolation methods were then used in subsequent analyses. The split-sample process was repeated only three times due to the large number of interpolation routines required to identify the optimal parameters for each interpolation method at each sampling percentage. There were 112 possible combinations of parameters for the three interpolation methods and every combination was used 3 times for each of the 5 sampling densities, resulting in a total of 1,680 interpolation routines to identify the optimal parameters for each interpolation method at each sampling percentage.

### 3.5 *Correlations*

From the aggregation of the 200 interpolation routines for each sampling density, the relationship between interpolation percent deviation, and distance to the nearest measurement, slope, and curvature were identified. The strength of association between the interpolation percent deviation and these three explanatory variables was individually quantified using the Spearman's rank-order correlation. This is a nonparametric version of the Pearson product-moment correlation, which was used since both the dependent and independent variables were not normally distributed (Mossa and McLean, 1997). Furthermore, the Spearman's rank-order correlation can capture any monotonic relationships (preservation of order) between variables, while the Pearson product-moment correlation is limited to assessing linear relationships.

The Spearman's rank-order correlation calculates the association by ranking the dependent and explanatory variables by magnitude. For example, the smallest percent deviation is given a ranking of one, the second smallest a ranking of two, etc. The same process is repeated for the explanatory variable in question. After both the variables are ranked, the differences between the paired ranks are calculated. For example, the percent deviation with a ranking of 1 is differenced with the ranking of the explanatory variable (e.g., curvature) that was queried at the location of the percent deviation with a ranking of 1. This is repeated for all ranks and the following formula is used to calculate the Spearman's rank-order correlation, rho ( $\rho$ ), where  $d_i$  = difference in paired ranks and  $n$  = number of cases.

$$\rho = 1 - \frac{6 \sum d_i^2}{n(n^2 - 1)}$$

A rho value of 1 corresponds to a perfectly positive monotone relationship between the two variables, indicating that an increase in one variable always corresponded with an increase in another variable. A rho value of -1 corresponds to a perfectly negative monotone relationship, indicating that an increase in one variable always corresponded with a decrease in another variable. A rho value of zero indicates no statistical relationship between the two variables.

### 3.6 *Median Percent Deviation Maps*

After repeating the split-sample and raster query processes 200 times, the median distance to the nearest measurement was calculated for every cell in the study area. Since the split-sample process was a random process, the median distance to the nearest measurement for every cell wasn't exactly the same, but instead showed a Gaussian distribution (Figure 13).

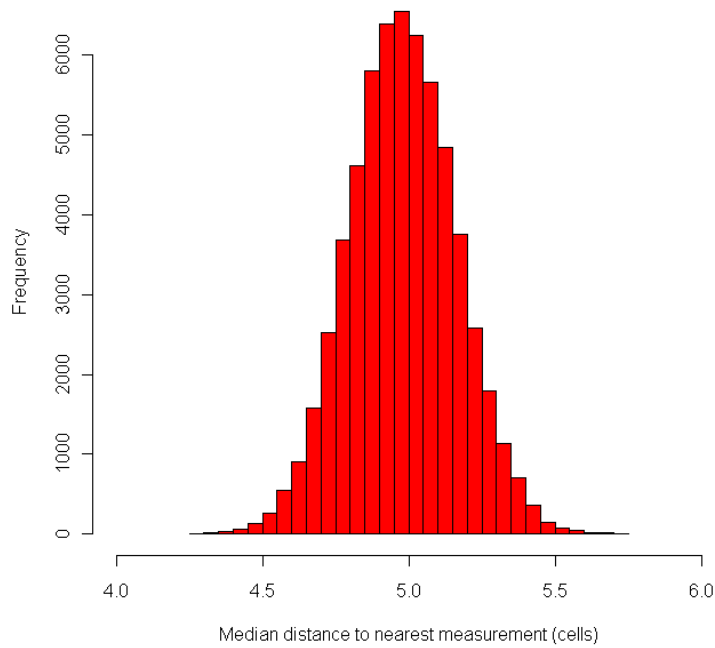


**Figure 13. Histogram of the median distance to the nearest measurement raster after 200 split-sample routines.**

After 200 iterations, the median distance to the nearest measurement for each cell ranged from 4.3 to 5.7 cells, with a median of 5 cells (Table 2).

**Table 2. Statistics of the median distance to the nearest measurement raster.**

<b>Statistic</b>	<b>Median Distance to the Nearest Measurement (cells)</b>
Minimum	4.3
1 <sup>st</sup> Quartile	4.9
Median	5.0
Mean	5.0
3 <sup>rd</sup> Quartile	5.1
Maximum	5.7

Since all cells had a similar median distance to the nearest measurement, the relationship between interpolation deviation and terrain characteristics was isolated and could be more

accurately identified. Furthermore, the percent deviation maps were used to address the limitations of global statistics, such as RMSE, in characterizing the accuracy of a non-stationary process.

## CHAPTER 4: RESULTS

The results of this research indicate that the accuracy of interpolation methods is related to the user-defined method parameters, sampling density, distance to the nearest measurement, and terrain characteristics. These results support previous studies that investigated the accuracy of interpolation methods in relationship to method parameters, sampling density and terrain characteristics. Previous research focused on topographic DEMs, and this study indicates that the accuracy of interpolating bathymetric DEMs produces similar results. Furthermore, by implementing the split-sample and raster query methodology 200 times and aggregating the interpolation deviations, a clear relationship between interpolation deviations and terrain characteristics is shown with median percent deviation maps that were not biased by the distance to measurements. Lastly, equations are presented that can be used to predict interpolation uncertainty for other areas of sparse measurements using distance to the nearest measurement and sampling density.

### *4.1 Optimal Interpolation Parameters*

The user-defined interpolation parameters were optimized using a brute-force methodology (See Ch. 3 Methodology). Identifying the optimal parameters ensured a reasonable analysis of the relationship between interpolation deviations and sampling density, distance to the nearest measurement, and terrain characteristics that would not be biased by poorly chosen interpolation parameters. The median percent deviation was calculated for each combination of parameters evaluated to determine the optimal parameters for each interpolation method. The importance of choosing appropriate interpolation method parameters is most significant when

interpolating across many cells due to a low sampling density, as the standard deviation of the median percent deviations from all combinations of evaluated parameters was the greatest at low sampling densities. Furthermore, the accuracy of IDW was the most sensitive method to the chosen parameters as indicated by having the greatest standard deviation of the median percent deviations from all combinations of parameters evaluated (Figure 14). The sensitivity of IDW accuracy to the user-defined parameters supports previous findings by Burrough and McDonnell (1998) and Akkala et al. (2010).

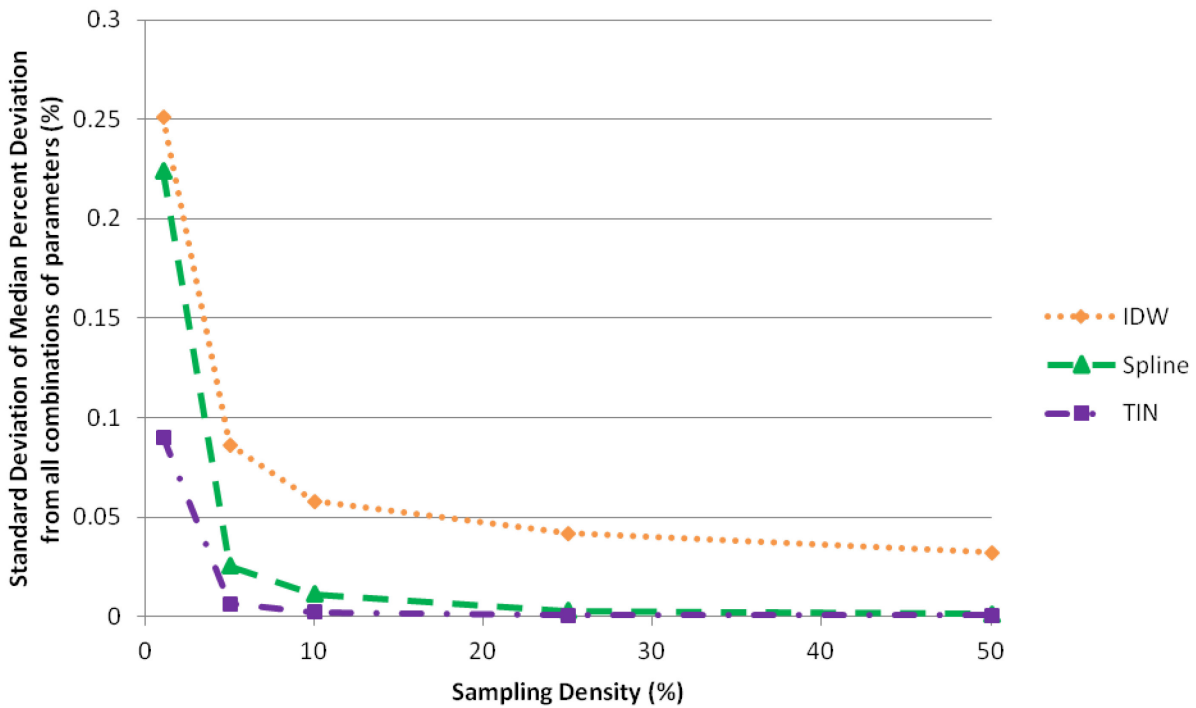


**Figure 14. Standard deviation of median percent deviations from all combinations of parameters evaluated for each interpolation method.**

In addition, the accuracy of spline interpolation was also found to be sensitive to the user-defined parameters. The sensitivity of spline accuracy to the parameters supports previous studies by Mitasova and Mitas (1993) and Cebecauer et al. (2002), which indicated that spline interpolation with a tension value set too low can create overshoots in areas of rapid changes of

gradient. Since spline interpolation is not constrained to the data range of the measurements used for interpolation, poorly-chosen parameters created significant artifacts with overshoots producing positive values when all input measurements were negative (Figure 15).

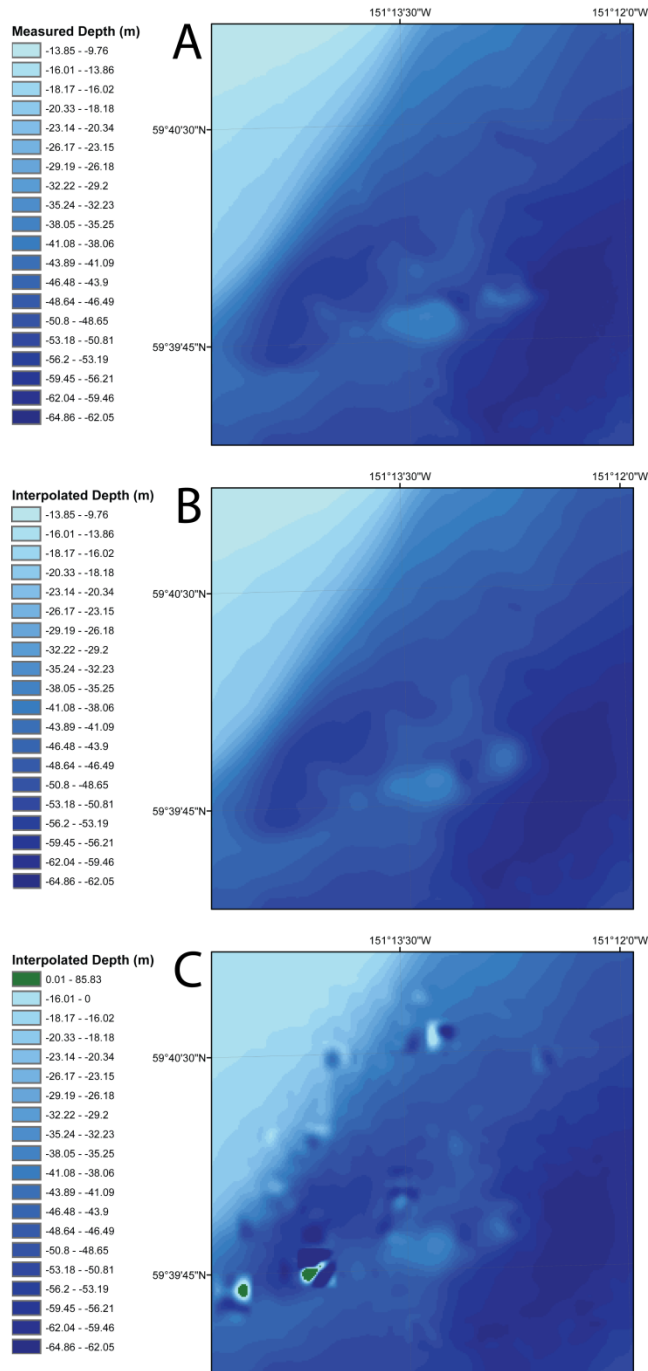


**Figure 15. Comparison of DEMs developed with spline interpolation with the optimal parameters and parameters that created artifacts.**

- A. Original depth measurement with no interpolation.**
- B. Spline interpolation using a random 1% sampling of depths with the optimal parameters (Spline Type = Regularized, Weight = 1, Number of Points = 100).**
- C. Spline interpolation using a random 1% sampling of depths with parameters that created artifacts (Spline Type = Tension, Weight = 0, Number of Points = 20; Note overshoots producing positive values).**

Lastly, there were insignificant differences in the conversion from TIN to raster using either linear or natural neighbor interpolation, especially at higher sampling densities. This research was most interested in extreme interpolation across many cells required at low sampling densities, and the optimal parameters identified when using a 1% sampling density were also found to be adequate to be used at the other sampling densities (Table 3).

**Table 3. Optimal interpolation method parameters identified using a 1% sampling density and used for subsequent analysis at all sampling densities.**

<b>Interpolation Method</b>	<b>Power</b>	<b>Search Radius</b>	<b>Spline Type</b>	<b>Weight</b>	<b>Number of Points</b>	<b>Raster Conversion Method</b>
IDW	2	Variable: 8 Points	_____	_____	_____	_____
Spline	_____	_____	Regularized	1	100	_____
TIN	_____	_____	_____	_____	_____	Linear

The optimal parameters identified for IDW and spline interpolation are related to the terrain of Kachemak Bay. For IDW, a higher power results in distant measurements having less influence, which produces a more detailed and less smooth surface. Conversely, a lower power results in distant measurements having greater influence, which produces a smoother surface. The optimal power identified was 2, which is relatively low and indicates that the measured depths of Kachemak Bay produced a smooth surface. For spline interpolation, the greater the number of points specified, the greater the influence of distant points and the smoother the surface. For regularized spline, a greater weight results in a smooth surface. The optimal parameters identified for spline interpolation, regularized spline type, weight of 1, and 100 points, also confirms the smooth bathymetry of Kachemak Bay.

#### 4.2 Interpolation Deviations & Sampling Density

After the optimal interpolation method parameters were identified, the split-sample process was repeated 200 times for each sampling density of original measurements (See Ch. 3 Methodology). As expected, the deviations of all three interpolation methods decreased when using more depth measurements (Figure 16). Many studies use a statistic such as RMSE as a global indicator of accuracy (Aguilar et al., 2005). However, this measure will be inflated in areas of deep water. Thus, the absolute median percent deviation was used instead, as it would not be as sensitive to the depth of water, and would allow for more accurate comparisons and applications to other study sites in deeper or shallower waters.

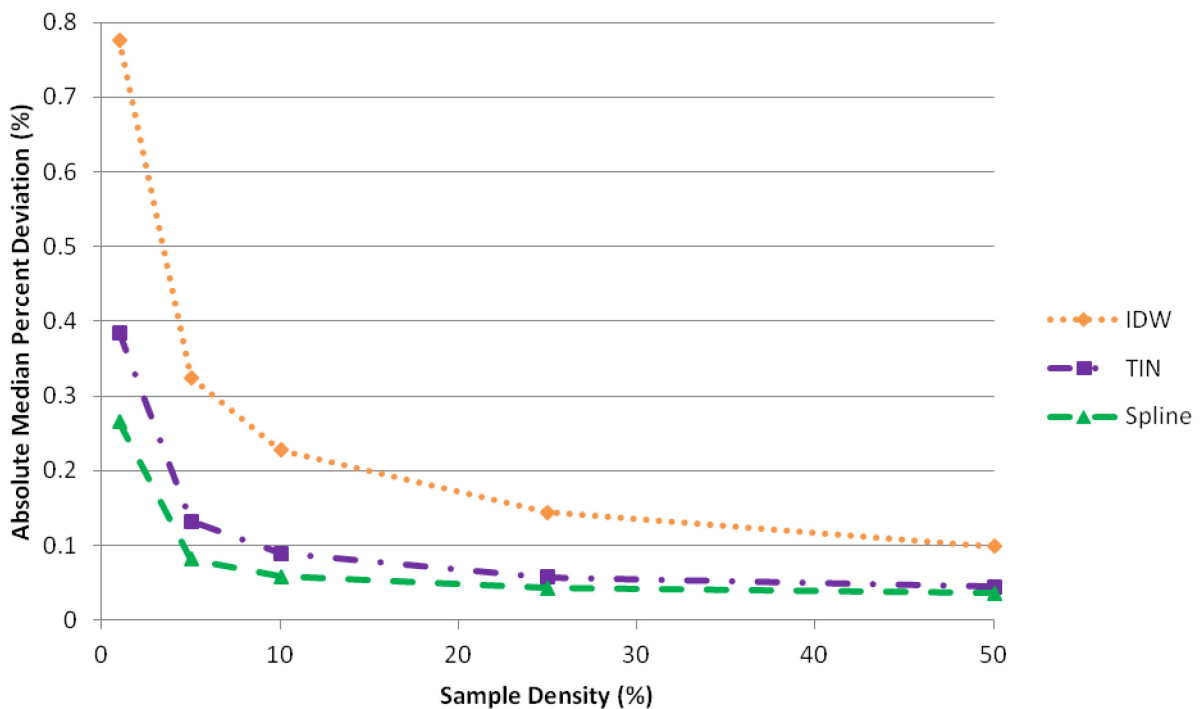


**Figure 16. Absolute median percent deviation as a function of sampling density.**

The largest differences in absolute median percent deviation between the three interpolation methods occurred when using 1% of the original measurements. As the percentage

of data used for interpolation increased, the median distance to the nearest measurement decreased, and the accuracy of all methods became more similar. Since the most notable differences between the interpolation methods occurred when using 1% of the original measurements, further analysis focused on this sampling density in order to determine the strengths and weaknesses of the various interpolation methods in relationship to terrain characteristics.

The differences between the three interpolation methods were very small when using 50% of the original measurements because there were typically measurements 1 cell away from a cell to be interpolated. Since the accuracy is comparable between the three methods at this sampling density, the choice of interpolation method should then be chosen based on computational and time resources. IDW is the fastest and least computationally intensive method and would therefore be adequate for most purposes when the median distance to measurements is approximately 1 cell. This finding supports previous studies that have indicated that IDW is comparable to much more complex statistical methods, such as kriging, when using higher sampling densities (Lloyd and Atkinson, 2002; Ali, 2004; Blaschke, 2004; Podobnikar, 2005; Chaplot et al., 2006; Liu et al., 2007). From Figure 16, the optimal sampling density can be identified for each interpolation method for this study area, depending on your required criteria of accuracy. The absolute median percent deviation for each method as a function of sampling density can be used to estimate interpolation uncertainty with a decaying power function (Table 4).

**Table 4. Equations to estimate interpolation uncertainty using the sampling density. Y represents the interpolation median percent deviation and X represents the percent sampling density.**

<b>Interpolation Method</b>	<b>Equation</b>	<b>R<sup>2</sup></b>
IDW	$y = 0.7676x^{-0.524}$	0.9997
Spline	$y = 0.2236x^{-0.512}$	0.9537
TIN	$y = 0.3502x^{-0.553}$	0.9866

However, the equations in Table 4 provide global estimates of uncertainty and assume the median distance to the nearest measurement (Table 5) for every cell, which typically is not the case with sparse depth measurements. The inadequacy of these equations is addressed by deriving equations to estimate interpolation uncertainty using distance to the nearest measurement in *Section 4.7*. The median percent deviation had the greatest decrease when the sampling density increased from 1% to 5%. This is likely because the median distance to the nearest measurement decreases from 5 cells to 2 cells with this 5-fold increase in sampling density. When the sampling density increases 5-fold from 5% to 25%, the median distance to the nearest measurement only decreases from 22.26 meters (2 cells in this study) to 10 meters (1 cell in this study; Table 5). This smaller decrease in the median distance to the nearest measurement corresponds with a similar smaller decrease in absolute median percent deviation in Figure 16 compared to the changes in deviation between the 1% and 5% sampling densities.

**Table 5. Relationship between sampling density and median distance to the nearest measurement.**

<b>Sampling Density (%)</b>	<b>Median Distance to the Nearest Measurement (m)</b>	<b>Median Distance to the Nearest Measurement (cells)</b>
1	50	5
5	22.26	~2
10	14.14	~1
25	10	1
50	10	1

### 4.3 Correlations

The split-sample and raster query processes were repeated 200 times at each sampling density with the optimal interpolation parameters. The distance to the nearest measurement, slope, and curvature rasters were queried for every interpolation percent deviation and the Spearman's correlations were calculated between the percent deviation and these explanatory variables. The positive correlation between the absolute percent deviation and distance to the nearest measurement shows a similar decreasing trend with higher sampling densities for all methods (Figure 17). This decreasing trend suggests that the distance to the nearest measurement is a better predictor of interpolation accuracy at low sampling densities, while at higher sampling densities, all unconstrained cells will be close enough to cells constrained by measurements that the interpolation deviation will be more related to the terrain, and especially curvature.

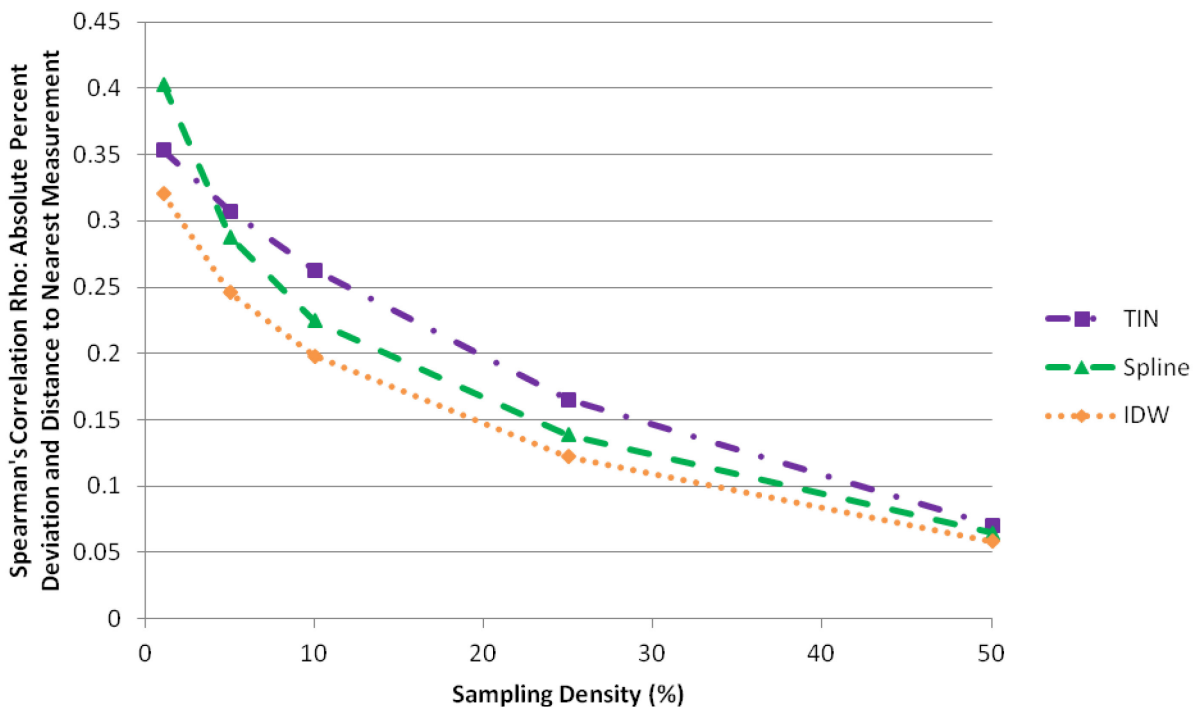


**Figure 17. Spearman's Correlation Rho between absolute percent deviation and distance to the nearest measurement as a function of sampling density.**

Absolute percent deviation and slope are also positively correlated with each other for all methods. However, IDW has a much stronger positive correlation with slope than TIN and spline (Figure 18). TIN and spline show similar decreasing trends with higher sampling densities, while IDW remains relatively constant at all sampling densities. IDW is most strongly correlated with slope as a result of the weighted-average algorithm, which can cause the interpolated depth to be much different than surrounding measured depths in areas of steep slopes.

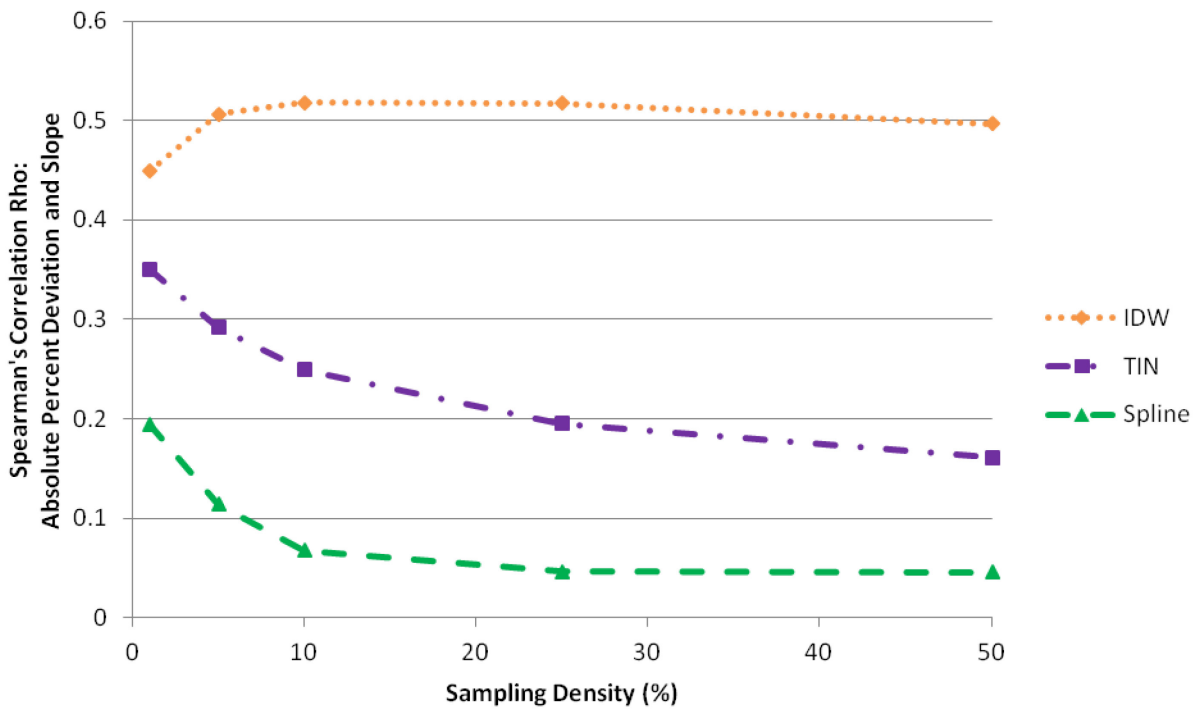


**Figure 18. Spearman's Correlation Rho between absolute percent deviation and slope as a function of sampling density.**

The correlation between absolute percent deviation and absolute curvature increases with greater sampling densities for all methods, but the correlations also indicate differences in the interpolation methods. TIN interpolation is the most strongly correlated with absolute curvature, followed by spline, and IDW is the least correlated with curvature (Figure 19).

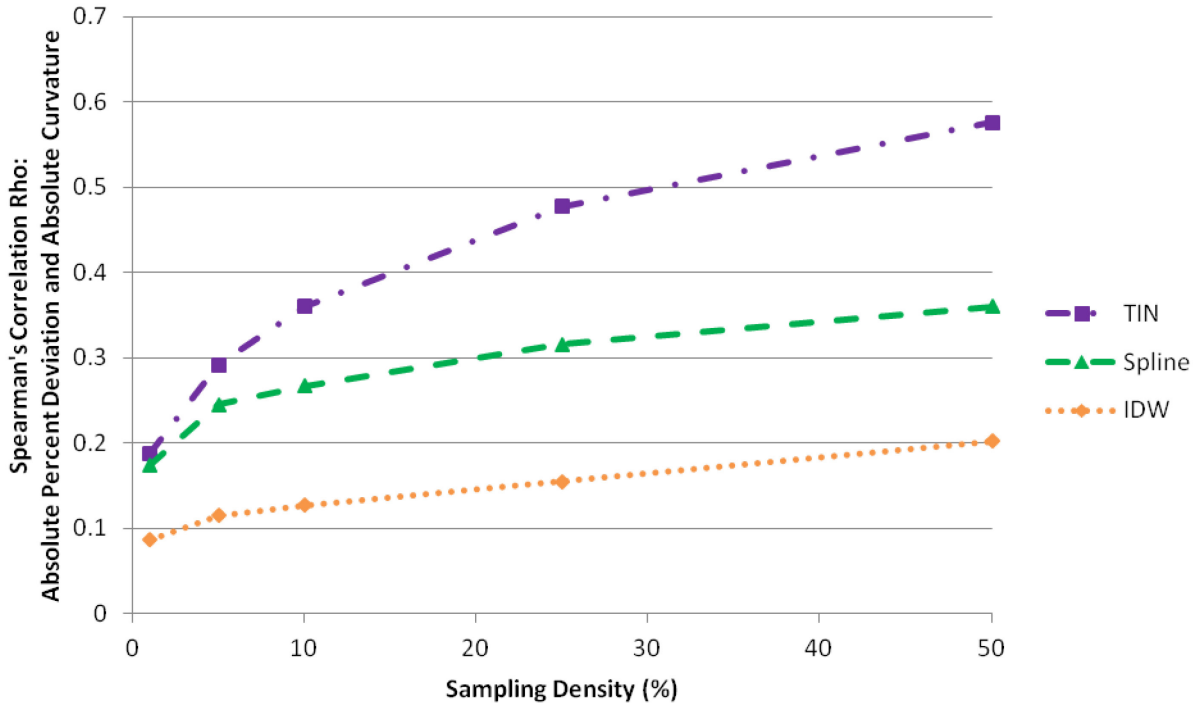


**Figure 19. Spearman’s Correlation Rho between absolute percent deviation and absolute curvature as a function of sampling density.**

When the signs of percent deviation and curvature are taken into account, the correlation shows the same trends as the absolute percent deviation and absolute curvature, but the correlation is greater for all methods (Figure 20). This reflects the relationship between whether the interpolated depths are deeper or shallower than the measured depths and the surface convexity or concavity of the measured depths.

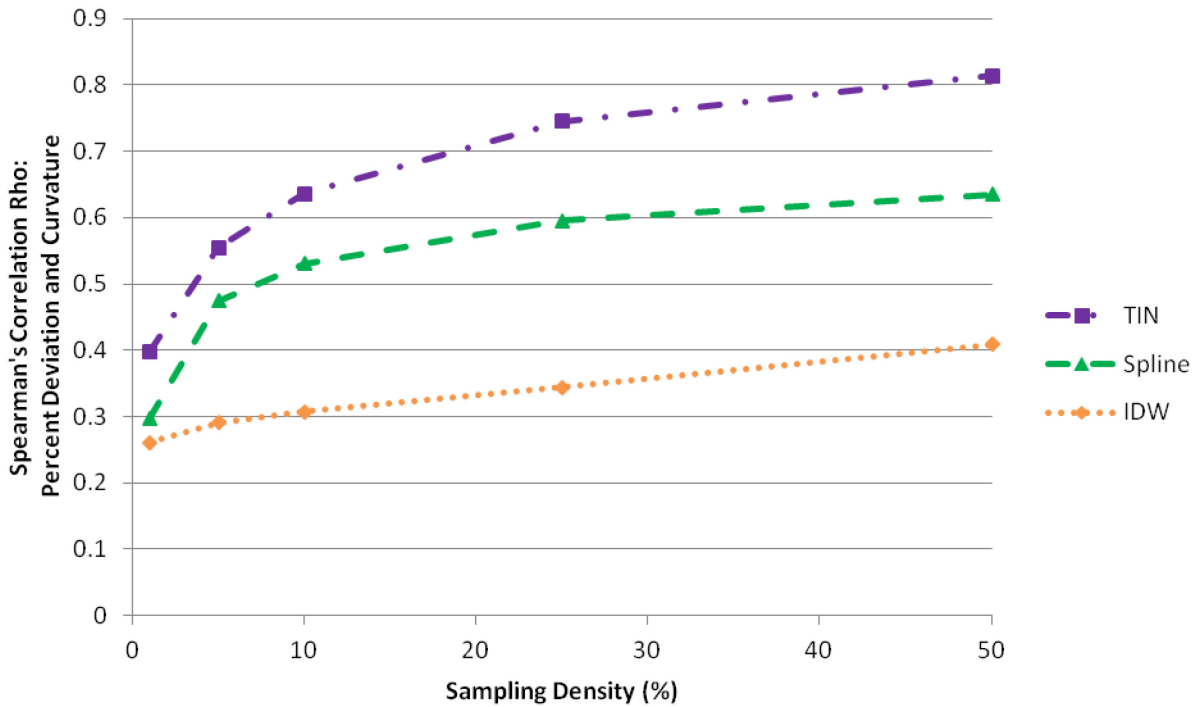


**Figure 20. Spearman’s Correlation Rho between percent deviation and curvature as a function of sampling density.**

A simple 2-D cartoon profile illustrates the relationship between TIN interpolation deviations and curvature, and how the sign of the interpolation deviation changes with convex and concave surfaces (Figure 21). Further analysis on the relationship between interpolation deviations and terrain characteristics is provided in the next two sections.

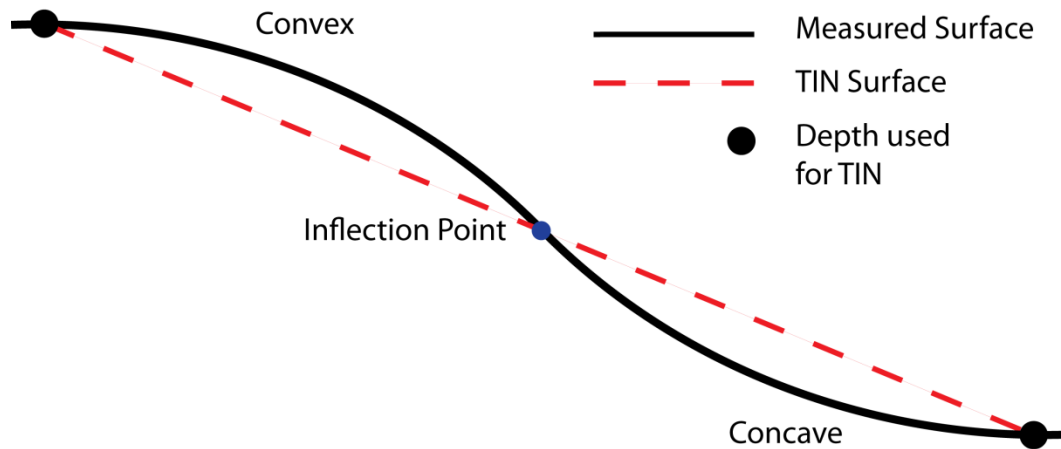


**Figure 21. 2-D cartoon profile showing relationship between the sign of TIN interpolation deviations and the surface curvature. TINs are typically deeper than the measured surface when the measured surface is convex and TINs are shallower than the measured surface when the surface is concave. TINs tend to become more accurate where the curvature of the surface is zero at the inflection point.**

#### 4.4 *Interpolation Deviations & Terrain*

The aggregated interpolation percent deviations after 200 split-sample routines using a random 1% sampling density were plotted as a function of slope and curvature, respectively. The absolute median percent deviation was calculated for binned slope values (Figure 22).

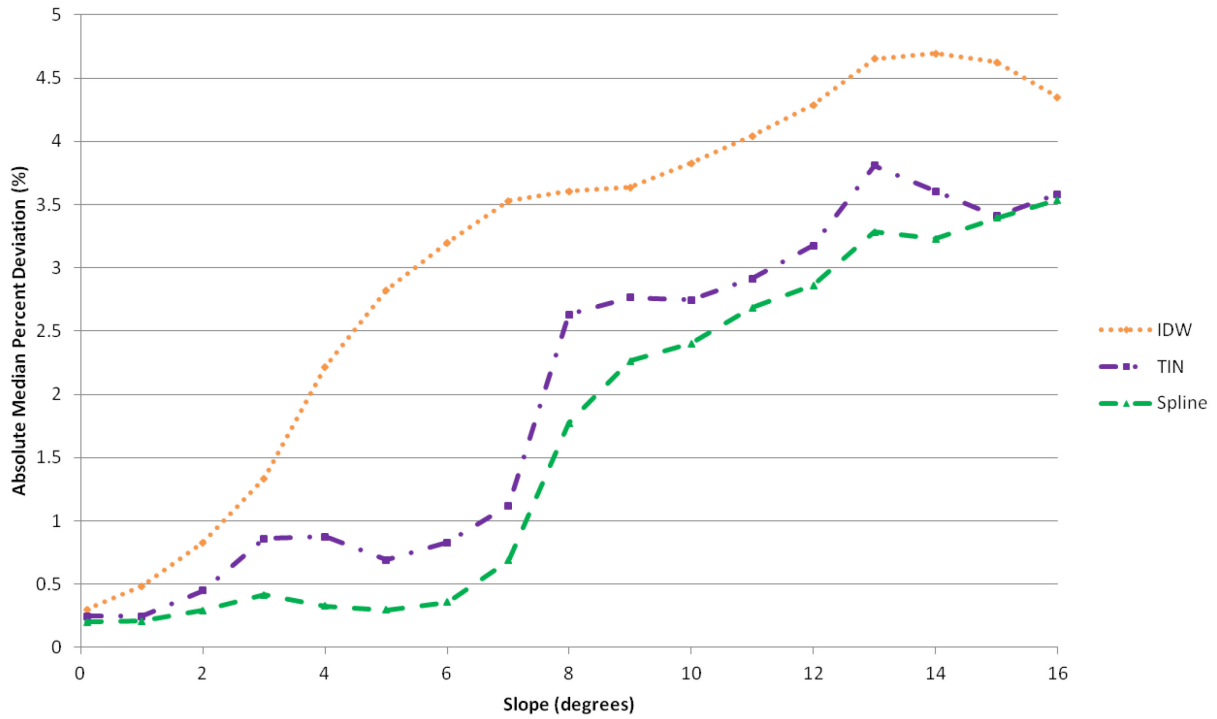


**Figure 22. Absolute median percent deviation as a function of slope using a 1% sampling density.**

Likewise, the median percent deviation was calculated for binned curvature values (Figure 23). Since one doesn't know the slope and the curvature of an area of the seafloor that requires interpolation due to a lack of depth measurements, these explanatory variables cannot be used to predict interpolation uncertainty. However, the graphs support the findings of the previous section that interpolation deviations are positively correlated with both slope and curvature for all methods.

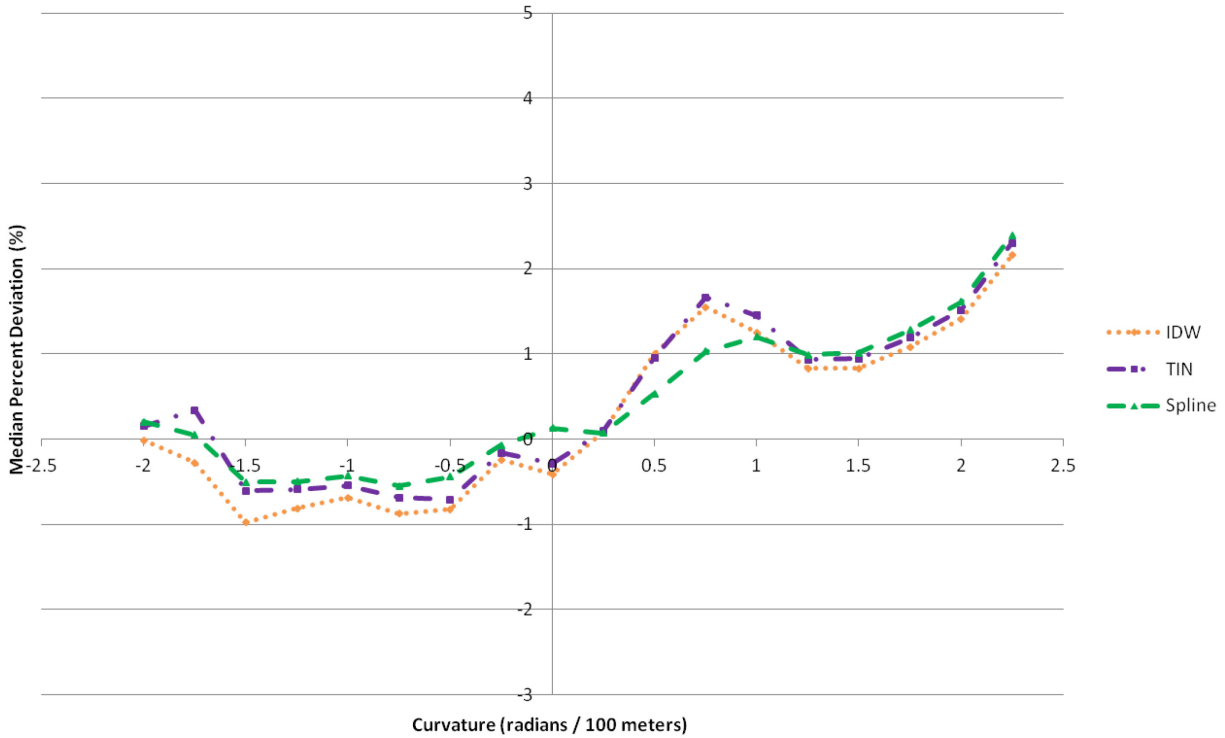


**Figure 23. Median percent deviation as a function of curvature using a 1% sampling density.**

#### 4.5 Median Percent Deviation Maps

The correlations and Figures 22 and 23 indicate an association between interpolation percent deviation and terrain characteristics. The absolute median percent deviation plotted as a function of sampling density in Figure 16 is a global statistic, and as previously mentioned, the interpolation percent deviation is highly non-stationary due to varied terrain. The interpolation median percent deviation maps address the issue of non-stationarity by highlighting clusters of higher deviations resulting from terrain without the bias of distance from measurements. At the lowest sampling density (1%), the percent deviations between the interpolated depths and the measured depths were the greatest and there were also the greatest differences between the interpolation methods. To show the effect of terrain on interpolation deviations, the median

percent deviation after 200 interpolation routines was calculated for every cell in the study area (Figures 24–26)

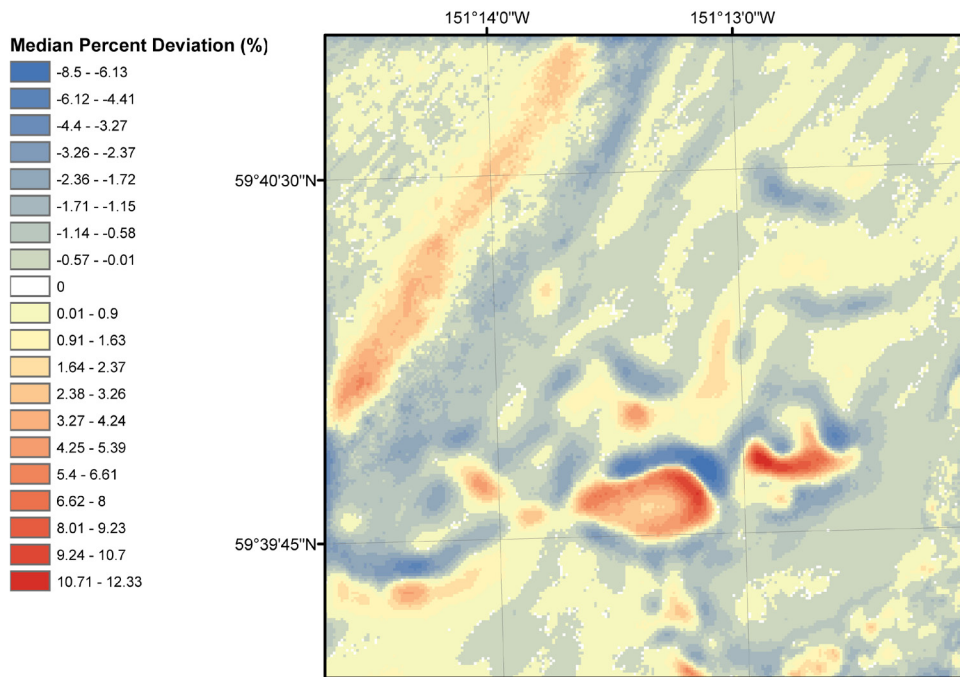


**Figure 24. Median percent deviation after 200 IDW interpolation routines using a random 1% sampling density.**

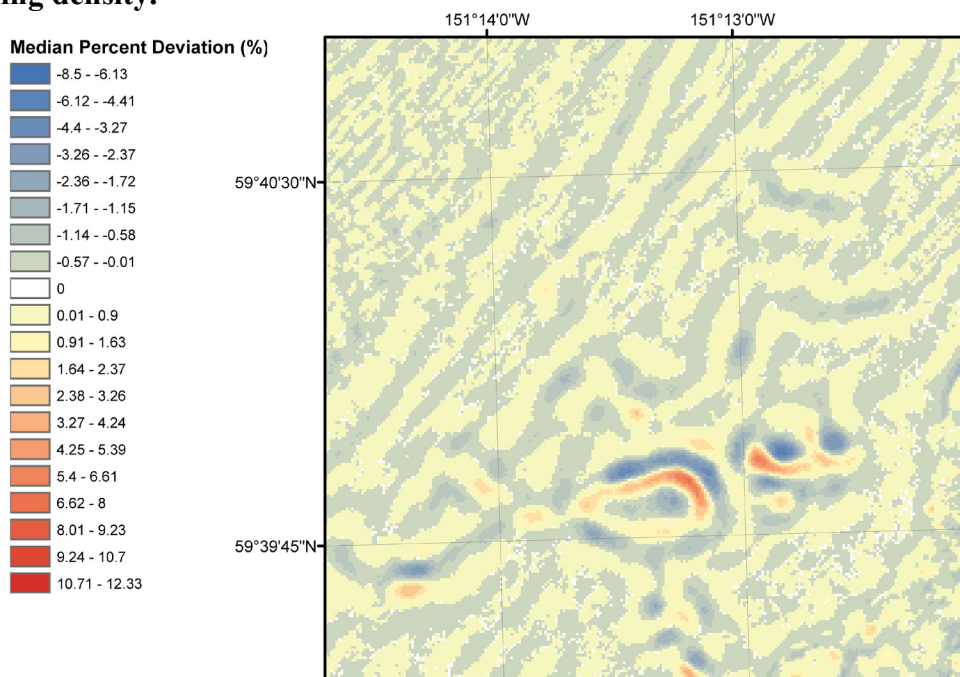


**Figure 25. Median percent deviation after 200 spline interpolation routines using a random 1% sampling density.**

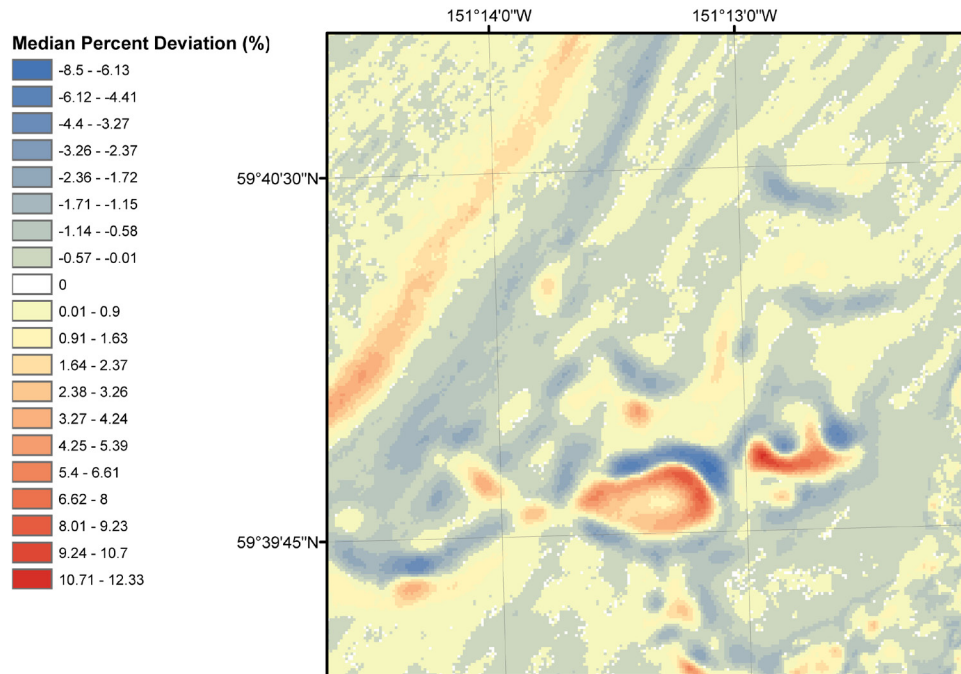


**Figure 26. Median percent deviation after 200 TIN interpolation routines using a random 1% sampling density.**

The median percent deviation rasters also indicate that spline interpolation is the most accurate of the methods, while IDW and TIN show comparable deviations. More importantly, all interpolation methods show a similar pattern of deviations that is strongly associated with the terrain. The slope and curvature rasters of the study area shown in Chapter 2 indicate that the interpolation deviations for all methods are greatest in areas of high curvature. Furthermore, the sign of the deviation is strongly correlated with the sign of the curvature, which describes if the surface is concave up or convex up. This relationship between terrain and interpolation deviations was further investigated in an inset area of variable slope and curvature (Figure 27, red outline).

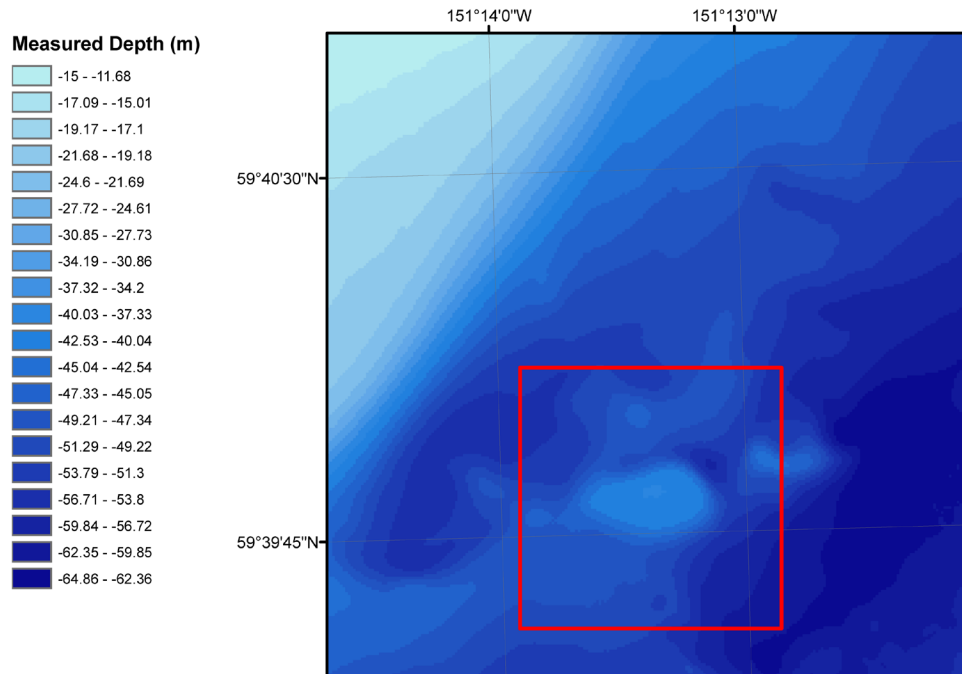


**Figure 27. The depth of an area of variable slope and curvature used to investigate the relationship between terrain and interpolation deviations is outlined in red.**

A profile across this area was then extracted from the slope (Figure 28), curvature (Figure 29), and median percent deviation rasters from each interpolation method (Figures 30–32) for further analysis.

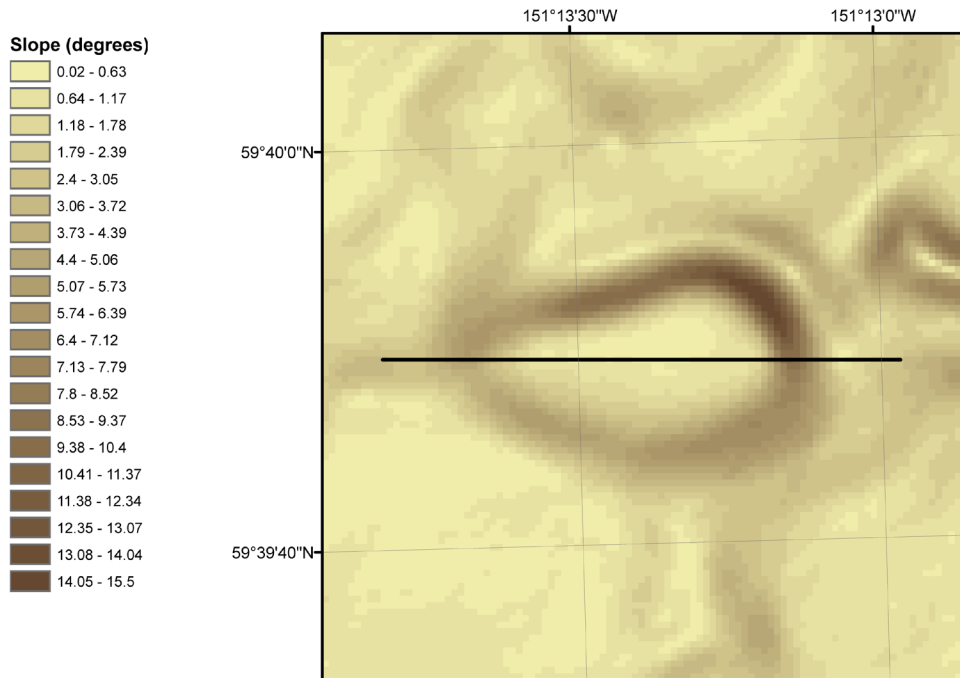


**Figure 28. Slope inset derived from measured depths.**

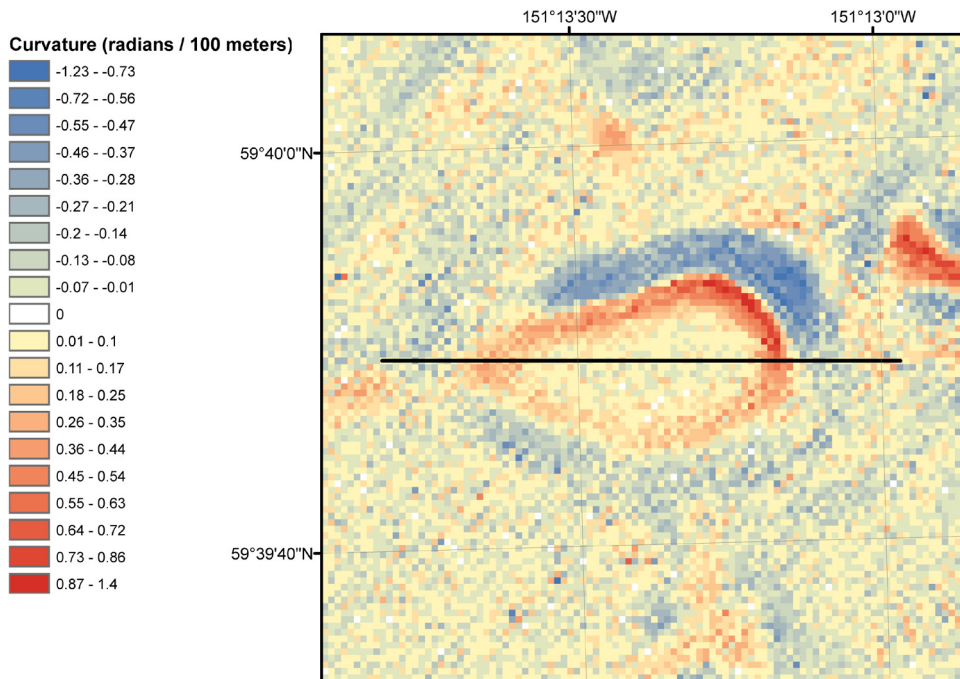


**Figure 29. Curvature inset derived from measured depths.**

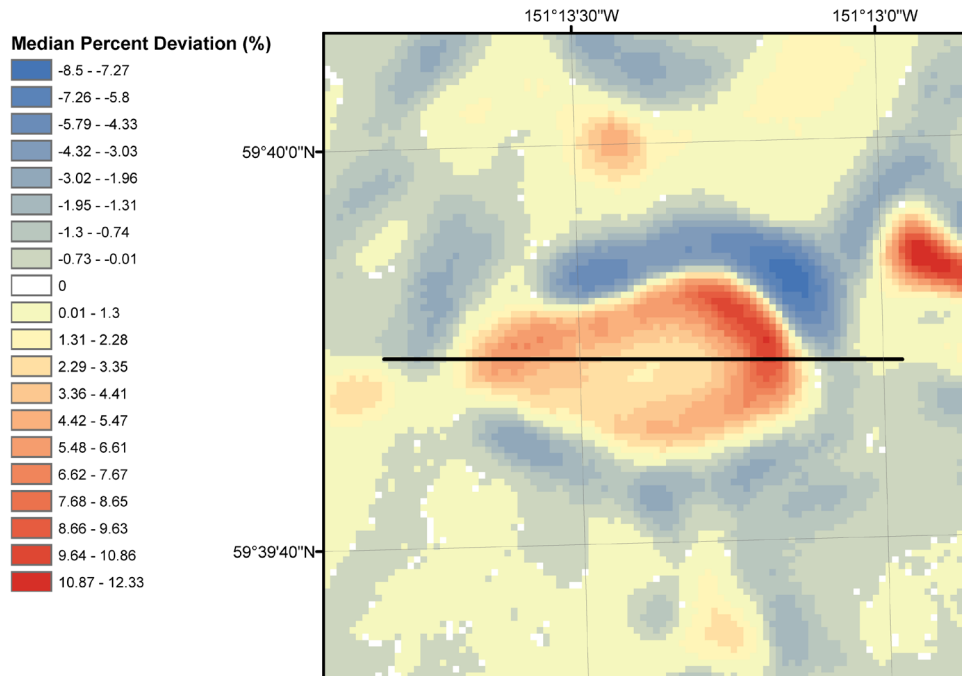


**Figure 30. Median percent deviation of inset area after 200 IDW interpolation routines using a random 1% sampling density.**

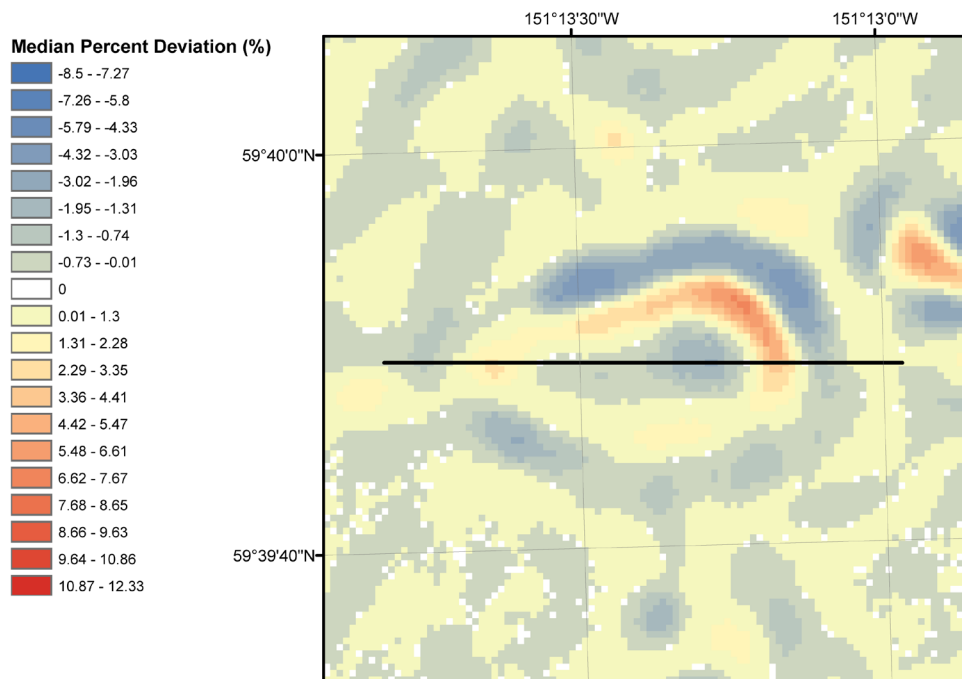


**Figure 31. Median percent deviation of inset area after 200 spline interpolation routines using a random 1% sampling density.**

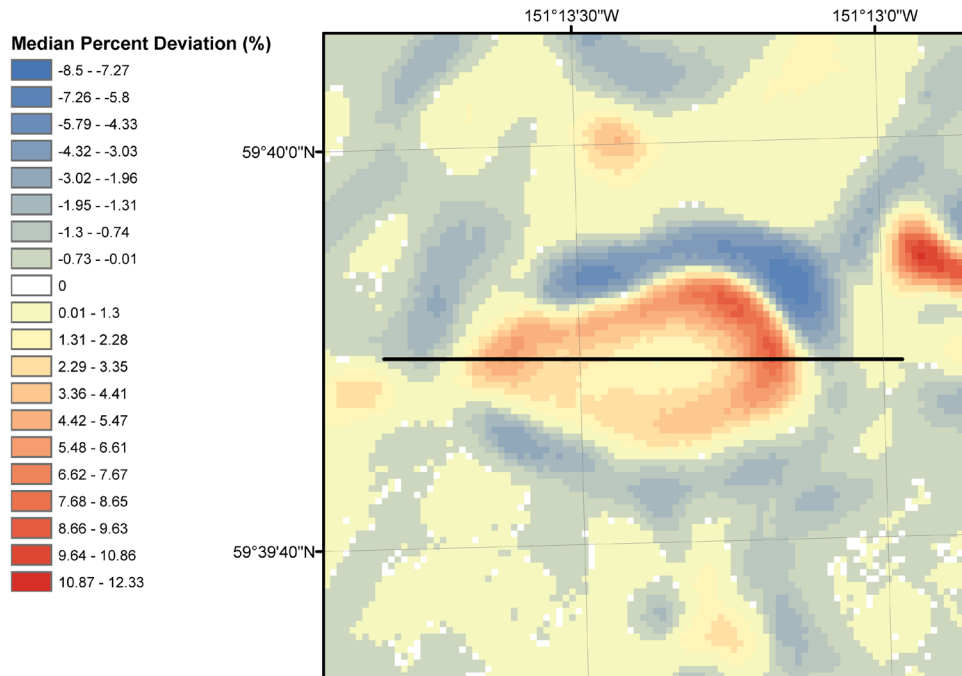


**Figure 32. Median percent deviation of inset area after 200 TIN interpolation routines using a random 1% sampling density.**

The largest median percent deviation for all methods is located at the area of highest curvature (Figures 33 and 34, red line). Likewise, the median percent deviation is close to zero for all methods where the curvature is also close to zero (Figures 33 and 34, black line).

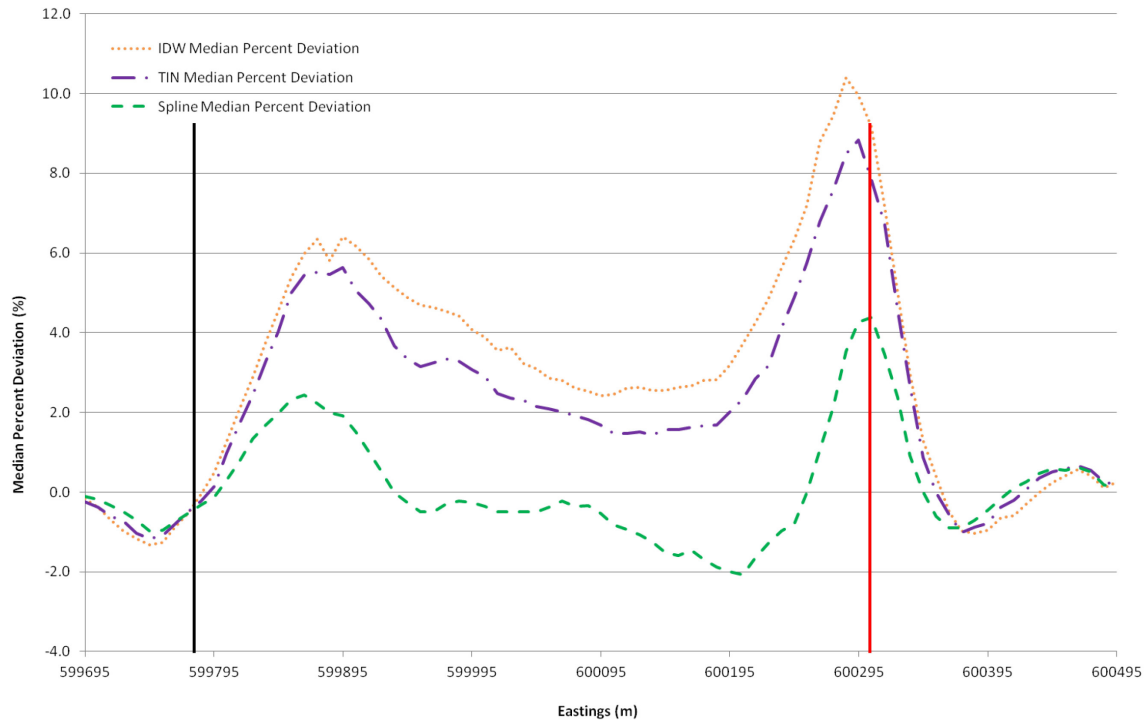


**Figure 33. Profile comparing median percent deviation from the three interpolation methods. The black line corresponds to a deviation close to zero for all methods and the red line corresponds to the largest deviation for all methods.**

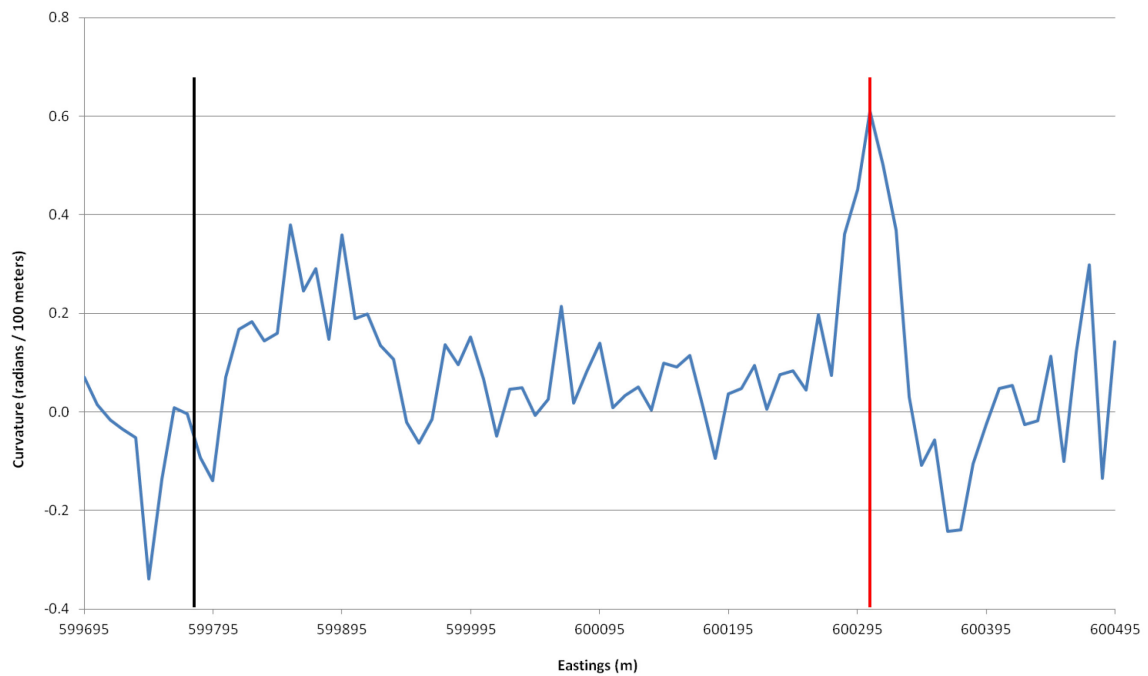


**Figure 34. Profile of the curvature derived from measured depths. The black line corresponds to a curvature close to zero (small deviation in Figure 33) and the red line corresponds to the highest curvature (greatest deviation in Figure 33).**

There is an obvious relationship between slope and curvature in that areas of higher slope are adjacent to areas of higher curvature. The location where the terrain changes from a flat area to an area of steep slope corresponds to an area of high curvature. However, it is evident that the location where the deviation is close to zero for all methods (black line), the slope is a modest 4 degrees (Figure 35). Furthermore, the location where the deviation is the greatest (red line) does not correspond to the highest slope. The correlations in *Section 4.3* and Figures 33 and 34 indicate that curvature is a better predictor of interpolation accuracy than slope.

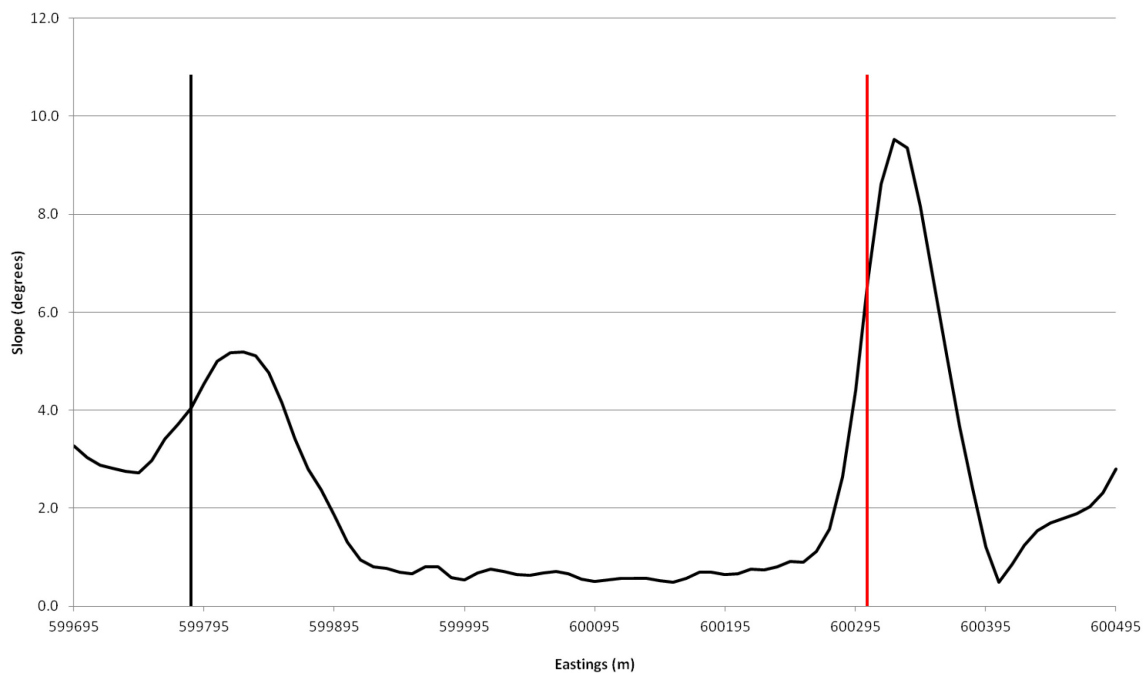


**Figure 35. Profile of the slope derived from measured depths. The black line corresponds to a small deviation for all methods in Figure 33, but not an area of low slope. The red line corresponds to the largest deviation for all methods in Figure 33, but not the location of greatest slope.**

The profiles of the median interpolated depths from which the previous median percent deviation profiles were calculated also highlight some notable properties of the methods. Since IDW uses a weighted-average algorithm, local maxima and minima will never be represented unless they have been sampled. Local maxima and minima near steep slopes will not be

accurately represented by IDW as local maxima are “pulled” down and local minima are “pulled” up by surrounding measurements. TIN is similar in that local maxima and minima will never be represented unless they are sampled and these areas will also either be too deep (local maxima) or too shallow (local minima). Lastly, spline exhibits “overshoots” near areas of high curvature as a result of the minimum curvature algorithm (Figure 36).

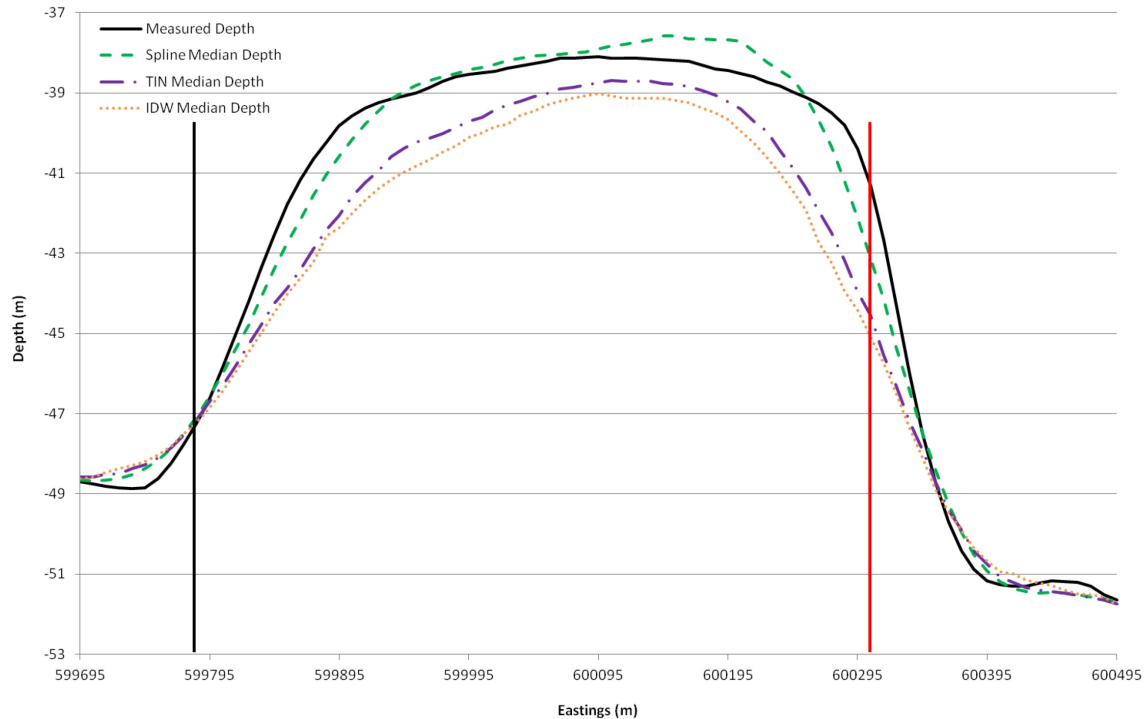


**Figure 36. Profiles of median interpolated depths after 200 iterations at a random 1% sampling density compared to the measured depths. All methods have small deviations at low curvature (black line) and large deviations at high curvature (red line). IDW and TIN produced local maxima that are “pulled” down and local minima that are “pulled” up. Spline can produce “overshoots” near areas of high curvature.**

#### 4.6 Interpolation Deviations & Distance to the Nearest Measurement

Since all interpolation methods evaluated in this study were exact interpolators, the interpolation deviations from the measured depths generally increase with greater distances from the nearest measurement used for interpolation. The same area and profile of varying slope and curvature used for analysis in *Section 4.5* was used again to illustrate the relationship between

interpolation accuracy and distance to the nearest measurement. In this area, 9 depth measurements along the profile were purposely used for interpolation solely to investigate the differences between the methods with greater distances from these measurements (Figure 37).

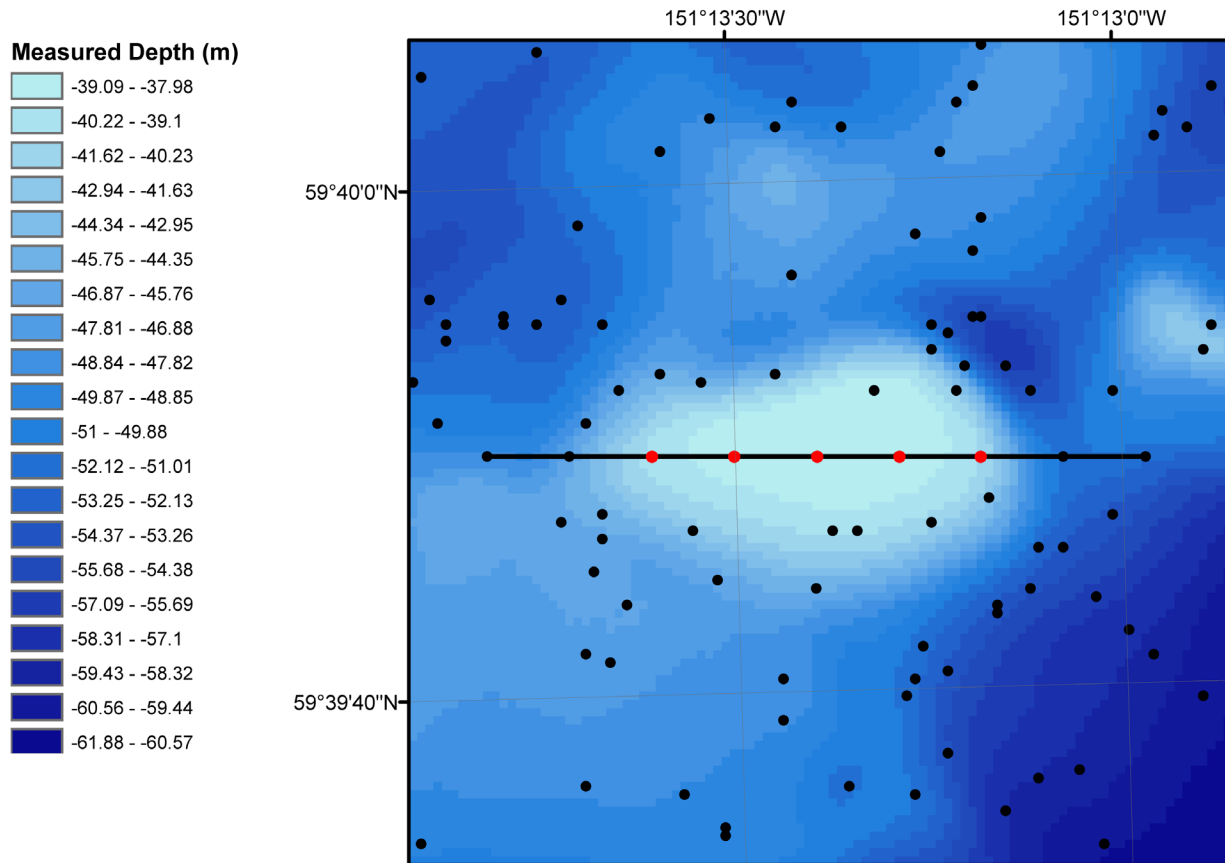


**Figure 37. Area of varying slope and curvature used to investigate the relationship between interpolation deviations and distance to the nearest measurements. Dots represent depths used for interpolation, with the red dots used for reference for later figures.**

IDW interpolation is sensitive to “bulls-eye” effects (Erdogan, 2009). Since IDW is an exact interpolator, the interpolated depths will also be the same as the original depth measurements used for interpolation. This can create “bulls-eyes” near depth measurements, especially when the depth measurement is much different in magnitude than surrounding depths (Figure 38).

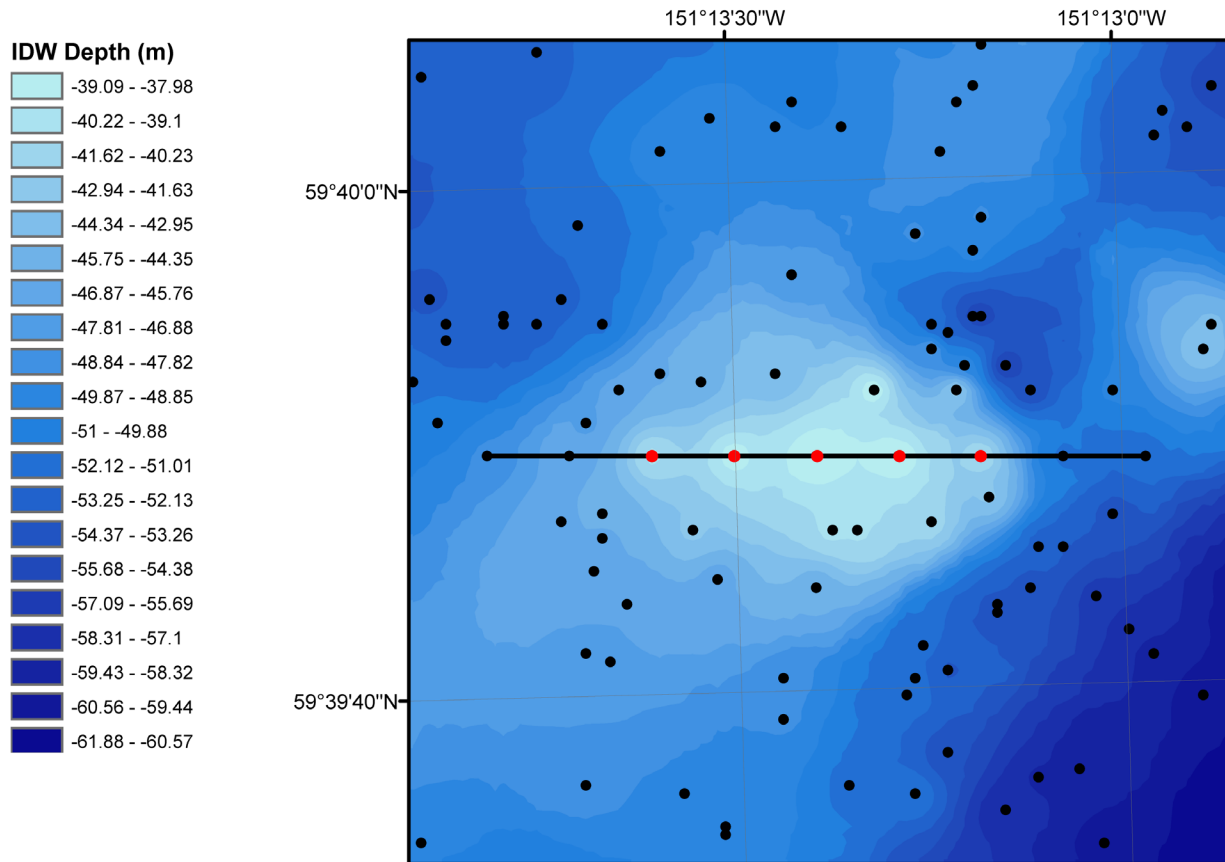


**Figure 38. IDW interpolated surface developed with depths at locations of black and red dots. Note the “bulls-eye” effect near red dots.**

In between the measurements in areas of high slope and curvature, IDW is often inaccurate due to the weighted average algorithm used for prediction (Figure 39).

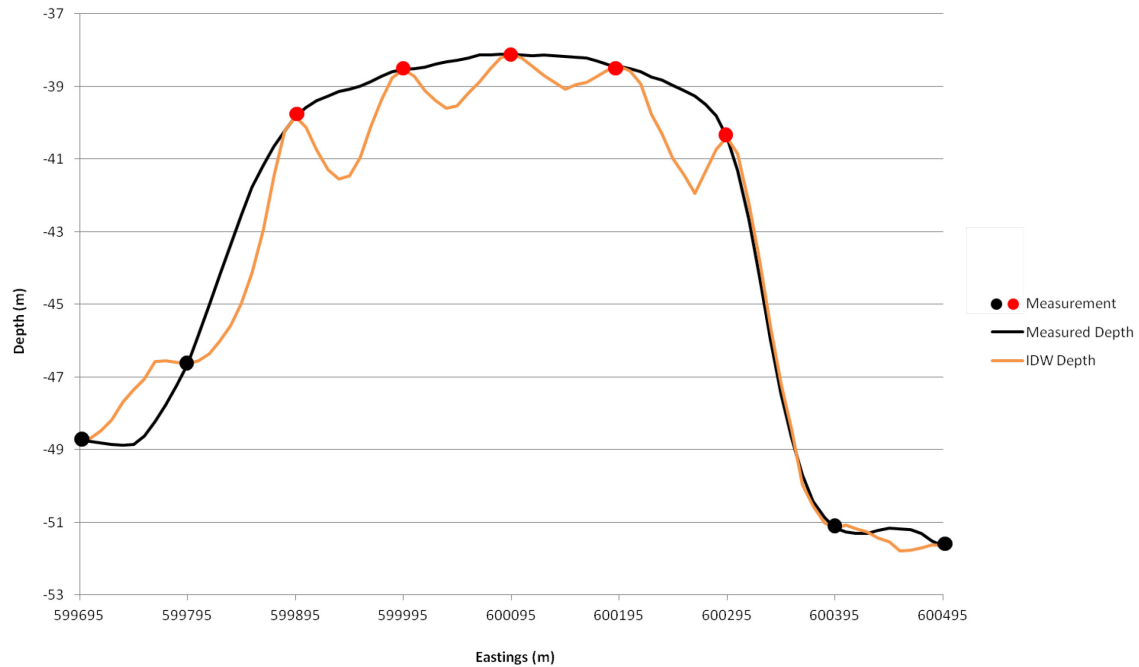


**Figure 39. Profile comparing IDW interpolated depths with the measured depths.**

While spline interpolation was found to be the most accurate method, a common issue are “overshoots” that occur at greater distances from measurements used for interpolation, particularly near areas of high curvature (Figure 40). The “overshoots” are caused by the minimum curvature algorithm used by spline interpolation.

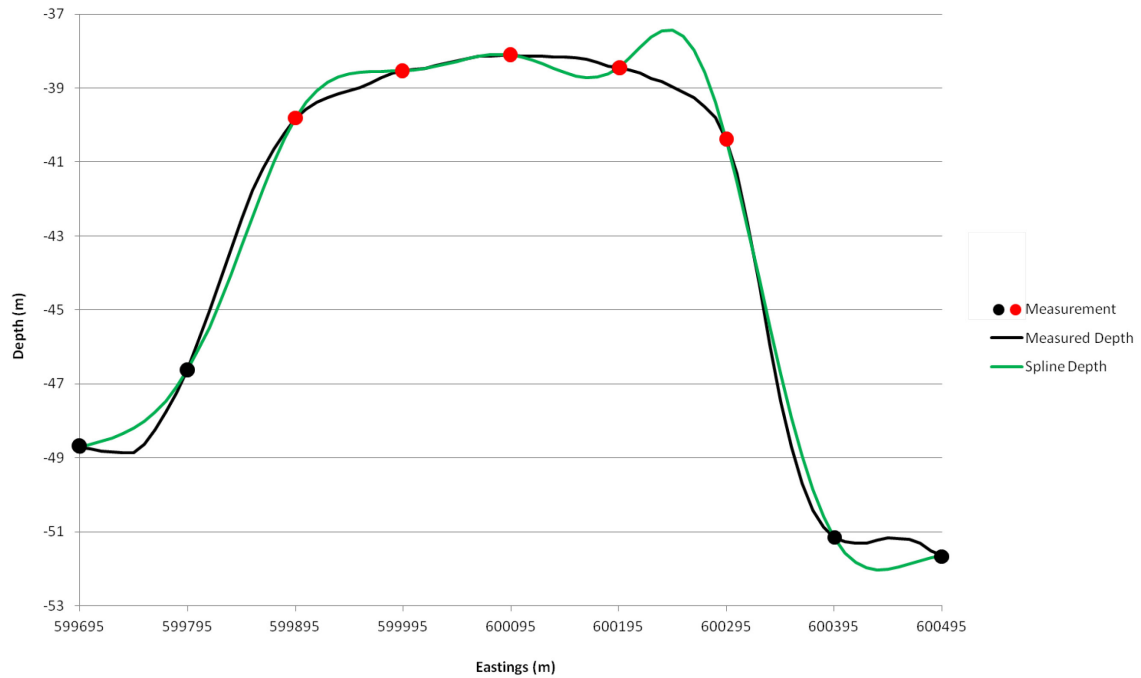


**Figure 40. Profile comparing spline interpolated depths with the measured depths.**

TIN surfaces are unrealistically flat and thus deviations are largest between measurements in areas of high curvature (Figure 41).

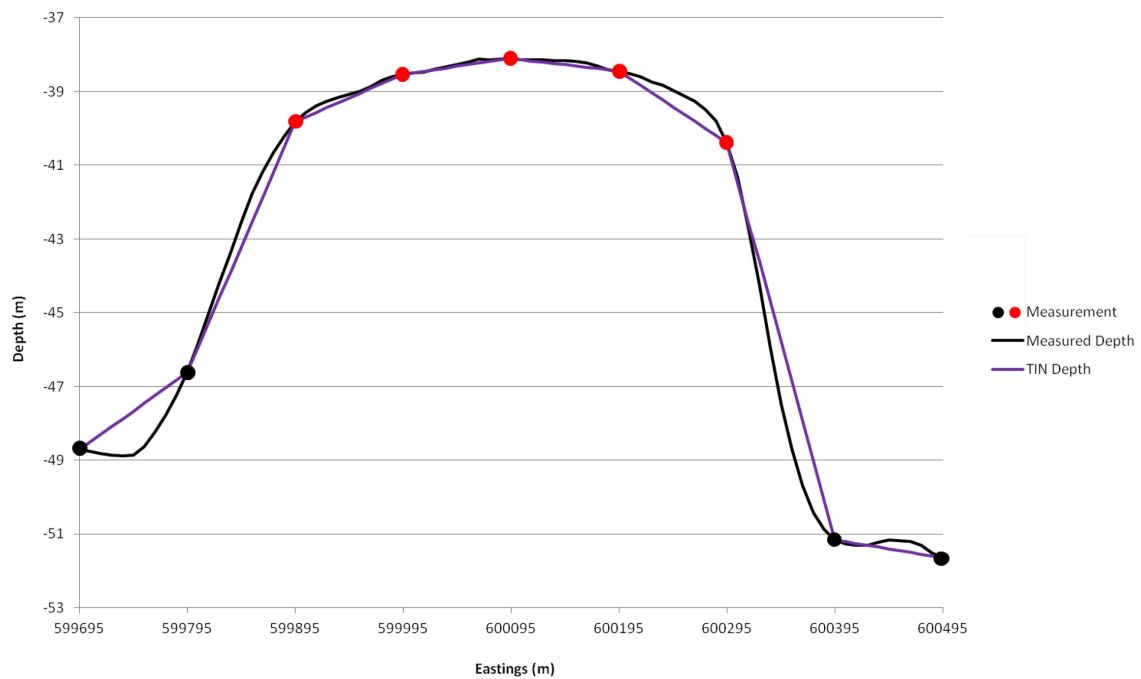


**Figure 41. Profile comparing TIN interpolated depths with the measured depths.**

#### 4.7 *Predictive Equations of Interpolation Uncertainty*

The slope and curvature of an area with no depth measurements is clearly unknown, and thus these variables cannot be used to predict interpolation uncertainty. Although slope and curvature can't be used for prediction, these explanatory variables were shown in previous sections to characterize the strengths and limitations of each interpolation method in estimating heterogeneous terrain.

The only known information when developing an interpolated DEM is the sampling density (ratio of cells constrained by depth measurements versus unconstrained cells at a given cell size), and the distance from an unconstrained cell to a depth measurement. Therefore, predictive equations of interpolation uncertainty were developed that could utilize this information. Figures 42 – 46 show the relationship between the absolute median percent deviation and the distance to the nearest measurement at the various sampling densities (1%, 5%, 10%, 25%, and 50%). The relationship between these variables diverges from the stable linear trend when the statistical sample size becomes too small (less than 300 deviations). At sample sizes less than 300, the absolute median percent deviation could be biased by the terrain at the locations of the deviations as it was calculated from a sample that was not representative of the median slope and curvature of the entire study area. Another reason for the divergence of the linear trend at greater distances from the nearest measurement is that the model of the semivariogram in Figure 5 indicates that depths in this study area separated by a distance greater than approximately 200 meters (20 cells) have little or no spatial autocorrelation and thus are not useful for interpolation.

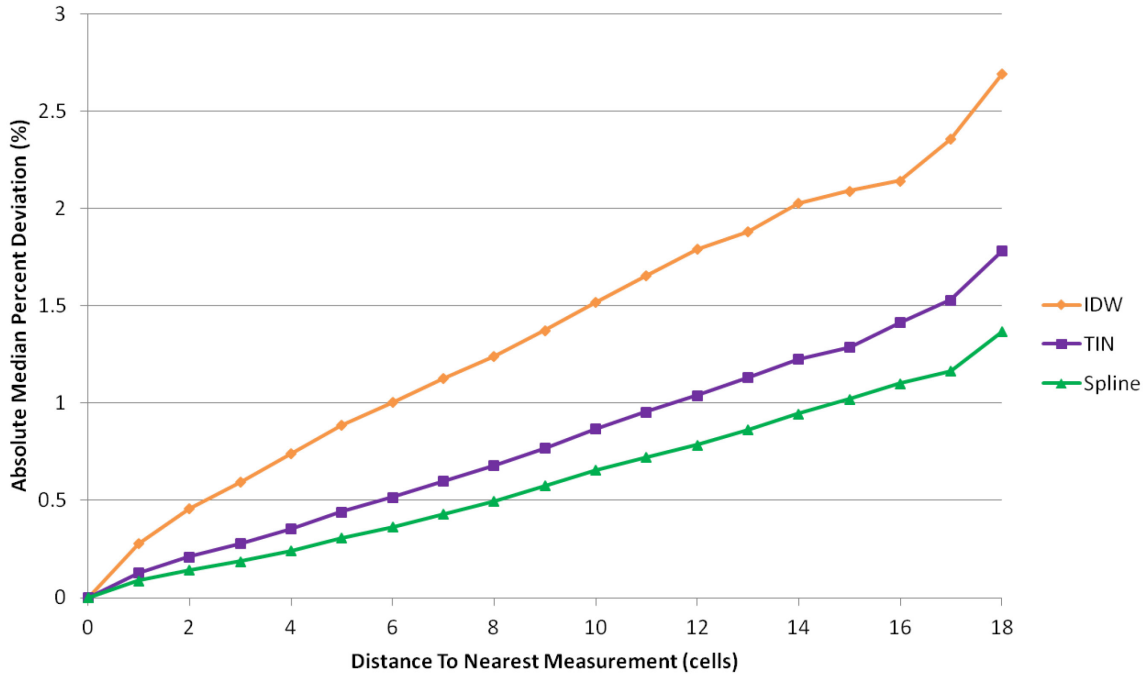


**Figure 42. Relationship between absolute median percent deviation and distance to the nearest measurement at a 1% sampling density. Beyond 18 cells the small sample size produces statistically insignificant results.**

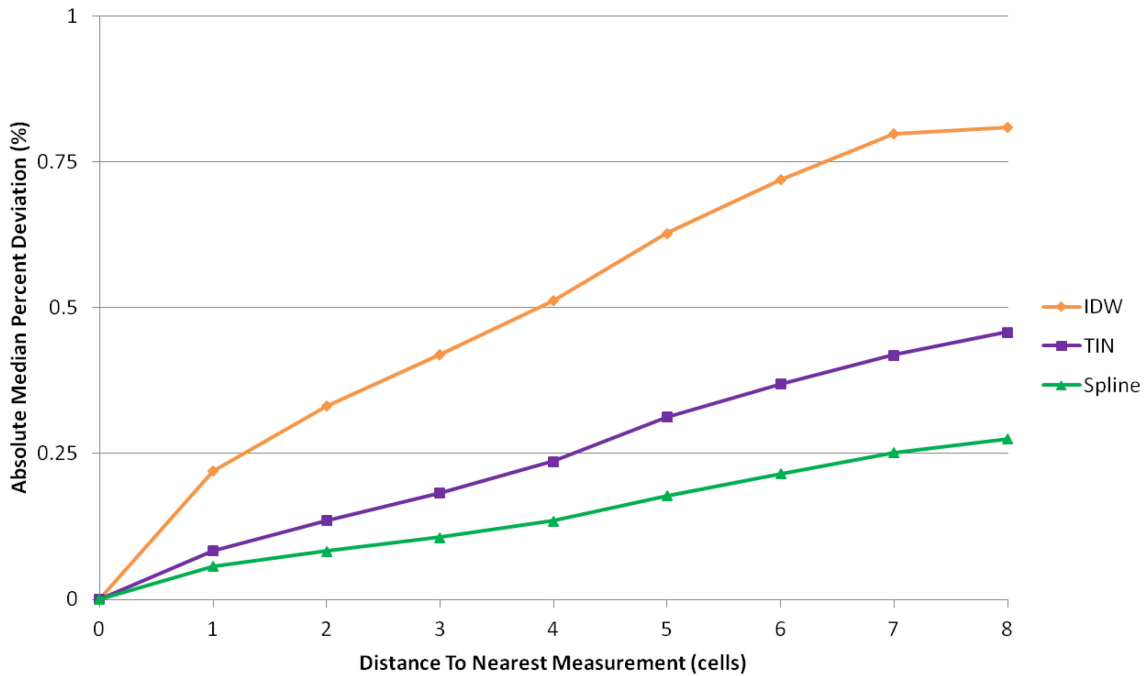


**Figure 43. Relationship between absolute median percent deviation and distance to the nearest measurement at a 5% sampling density. Beyond 8 cells the small sample size produces statistically insignificant results.**

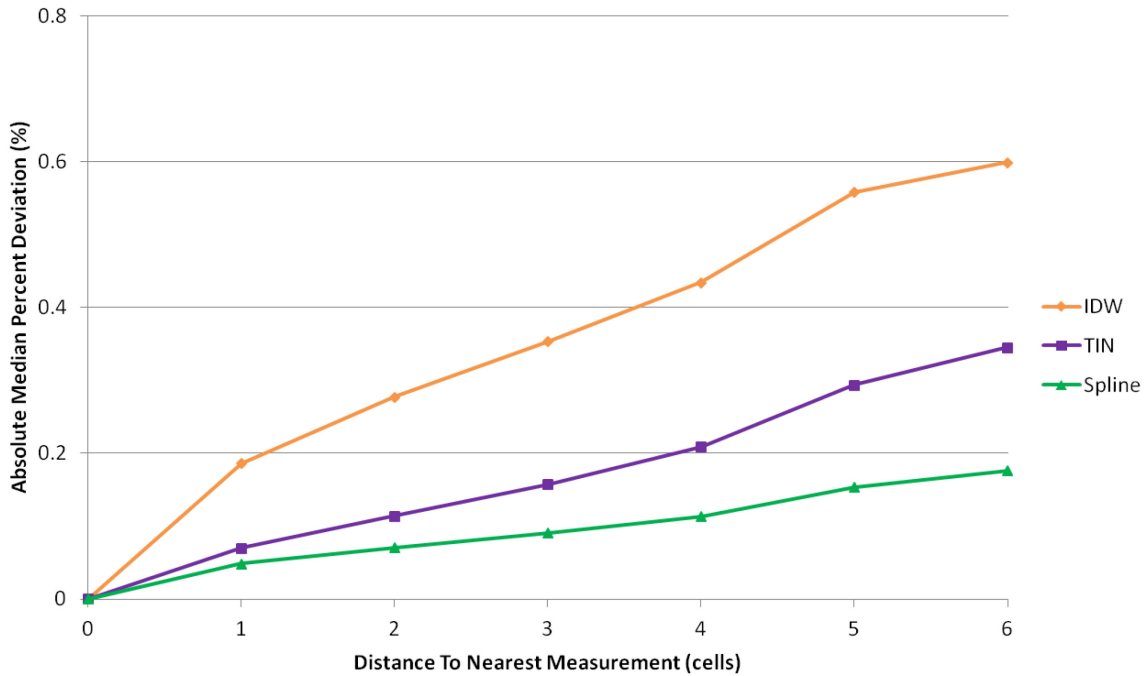


**Figure 44. Relationship between absolute median percent deviation and distance to the nearest measurement at a 10% sampling density. Beyond 6 cells the small sample size produces statistically insignificant results.**

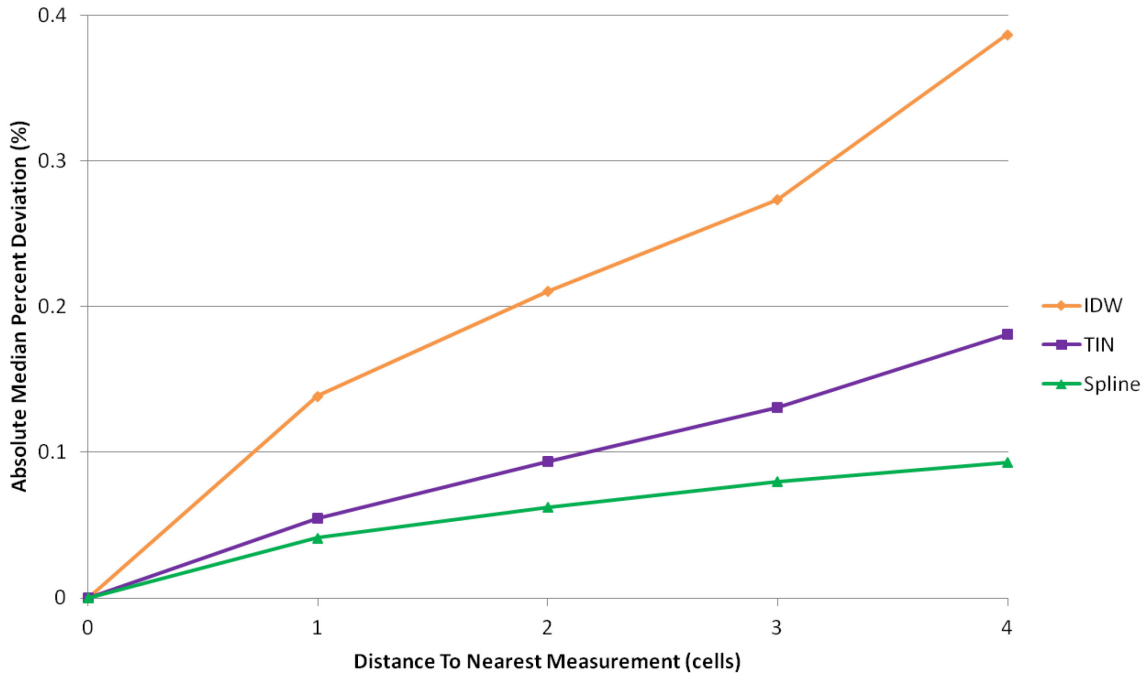


**Figure 45. Relationship between absolute median percent deviation and distance to the nearest measurement at a 25% sampling density. There were no interpolated cells where the distance to the nearest measurement was greater than 4 cells.**

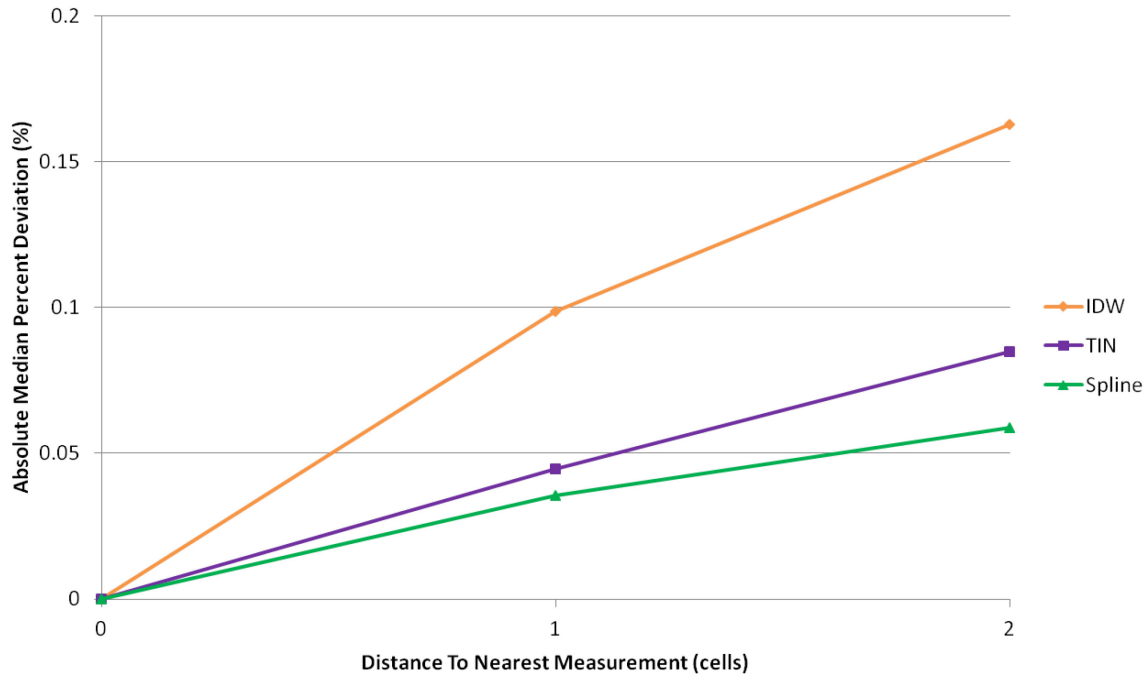


**Figure 46. Relationship between absolute median percent deviation and distance to the nearest measurement at a 50% sampling density. Beyond 2 cells the small sample size produces statistically insignificant results.**

As the sampling density becomes greater, the distances to the nearest measurement are constrained to closer distances. Also, while all five graphs show a linear trend, the slope of the regression line decreases with higher sampling densities (Note differences in Y-axis units). The differences in regression slope signify that it is not only the distance to the nearest measurement to an unconstrained cell that determines the accuracy of the interpolated cell, but that the accuracy is also related to the sampling density. Even if the distance to the nearest measurement is the same when using different sampling densities, the distance to the next nearest measurement that is also used for interpolation will likely be closer at higher sampling densities, and thus more similar to the depth to be interpolated, resulting in smaller interpolation deviations.

Therefore, both the sampling density and distance to the nearest measurement were used together to predict the interpolation uncertainty on a cell-to-cell basis. The statistically insignificant results due to low sample size were eliminated for each sampling density and then linear regression equations were derived using ordinary least squares regression for each sampling density with the y-intercept set to zero since all three methods are exact interpolators (Table 6). If the sampling density is between one of the percentages evaluated in this study, a weighted-average of the two closest linear regression equations provided in Table 6 could be calculated to predict the median percent uncertainty. These regression equations are best-suited for Kachemak Bay and for other areas of similar topography. However, they can be applied to other study areas with the caveat that these equations will underestimate interpolation deviations in areas of higher in magnitude curvature than Kachemak Bay, and overestimate interpolation deviations in areas of lower curvature.

**Table 6. Regression equations modeling interpolation percent uncertainty (y) as a function of distance to the nearest measurement in cells (x) for various data densities.**

Interpolation Method	Sampling Density (%)	Regression Equation	R <sup>2</sup>
IDW	1	y=0.1462x	0.9774
IDW	5	y=0.1162x	0.9256
IDW	10	y=0.109x	0.9497
IDW	25	y=0.0976x	0.9724
IDW	50	y=0.0848x	0.9819
Spline	1	y=0.068x	0.9884
Spline	5	y=0.0354x	0.9895
Spline	10	y=0.0302x	0.9759
Spline	25	y=0.0259x	0.9139
Spline	50	y=0.0306x	0.9822
TIN	1	y=0.0893x	0.9906
TIN	5	y=0.0599x	0.9921
TIN	10	y=0.0565x	0.9911
TIN	25	y=0.0453x	0.9933
TIN	50	y=0.0429x	0.9988

## CHAPTER 5: DISCUSSION & CONCLUSIONS

The findings of this research support previous studies on the accuracy of interpolation methods used to develop DEMs. The interpolation deviations for all methods were positively correlated with distance to the nearest measurement, slope, and curvature. As expected, higher sampling densities resulted in greater accuracy for all interpolation methods. The split-sample methodology has been used in numerous previous studies that investigated interpolation accuracy (e.g., Desmet, 1997; Lloyd and Atkinson, 2002; Smith et al., 2003; Erdogan, 2009). However, these studies did not repeat the random split-sample process to use different measurements for interpolation and evaluation. Furthermore, the aggregation of the 200 split-sample routines allowed for a more comprehensive investigation of the relationship between interpolation accuracy and terrain characteristics that was not biased by the distance to the nearest measurement. The results from this study highlight important strengths and weakness of three commonly-used interpolation methods in areas of heterogeneous terrain with varied slope and curvature values.

Spline was found to be the most accurate interpolation method at all sampling densities (1%, 5%, 10%, 25%, and 50%), followed by TIN, and IDW was the least accurate. The largest differences in accuracy between the methods occurred at the lowest sampling density (1%). When using 50% of the depths, there was typically a measured depth 1 cell away from an unconstrained cell to be interpolated and thus there were insignificant differences between the three interpolation methods. A sensible question that should be asked by any DEM developer is: “What is the acceptable level of interpolation accuracy?” The answer clearly depends on the purpose of the DEM. If the DEM will be used simply for visualization for outreach activities,

any method would most likely be acceptable, but spline would be preferred because of its smooth, visually appealing surfaces. Furthermore, if there is only a minimal loss of accuracy when using 10% of the available data, it may be more efficient to only use this data subset and apply an interpolation method to minimize computational resources. This is especially true when using dense lidar data that can require terabytes in computer storage. Regardless of the desired accuracy of the interpolated DEM, an accompanying estimate of DEM accuracy is extremely beneficial. People who develop or use DEMs may forget that the “M” in DEM stands for model and may not even consider how close the model mimics reality. The findings of this research can be used to develop uncertainty surfaces to accompany DEMs. Uncertainty surfaces would be extremely valuable for people using DEMs for other modeling purposes, such as tsunami propagation and inundation, to aid in quantifying the propagation of uncertainty (Hare et al., 2011). An uncertainty surface would ideally encompass both source measurement and interpolation uncertainty.

Based on the findings of this research, the following recommendations are provided on using an interpolation method to develop a DEM and estimating the uncertainty introduced by interpolation. First, determine the horizontal resolution and the desired vertical accuracy based on the intended purpose of the DEM. Next, calculate the sampling density by comparing the ratio of cells constrained by measurements to unconstrained cells at the chosen cell size. If greater than 25% of the cells are constrained by measurements, then the median distance to the nearest measurement will be approximately 1 cell away and the accuracy of spline, IDW, and TIN will be comparable. If the sampling density is less than 25%, then spline interpolation will provide a significantly more accurate DEM. Next, for every cell in the DEM, calculate the distance to the nearest measurement using the ArcGIS “Euclidean Distance” tool or a comparable method and

convert the distance from map units to cells by dividing the distance by the cell size. After selecting an interpolation method to develop the DEM, the interpolation percent uncertainty can be estimated for each cell by using the appropriate equation in Table 6. If the sampling density falls between two sample densities evaluated in this study, calculate a weighted-average of the interpolation percent uncertainty provided by the two bounding sample densities.

The uncertainty of interpolation methods is a complex subject with many important aspects not able to be adequately addressed within the scope of this study. There were numerous assumptions that were made in this research that should be considered when analyzing and applying the results. Most significantly, the uncertainty inherent in the source measurements was ignored, and the original measured depths were considered a “true” depiction of reality. This simplistic view was required to quantify interpolation deviations and to develop predictive equations of interpolation uncertainty, but it would be worthwhile to investigate the propagation of measurement uncertainty into interpolation uncertainty.

Another possible limitation is that the results obtained from this study may not be directly applicable to other areas with different terrain. Kachemak Bay, AK was considered an ideal study area to investigate the accuracy of interpolation methods as the terrain varied from areas of constant depths to areas of rapidly changing depths. The heterogeneous terrain should allow for the results of this study to be applicable to many other locations. However, if the results found at Kachemak Bay were applied to another study area that was relatively flat with low curvature, the provided estimates of interpolation uncertainty would be overestimated. Likewise, if another area had higher curvature values, then the estimates of interpolation uncertainty provided in this study would be underestimated. However, the variability of terrain between sparse depth measurements can't be known. Since the Kachemak Bay study area had varied terrain,

estimating interpolation uncertainty using only the distance to the nearest measurement and sampling density with the equations provided in Table 6 should produce reasonable results for a wide range of terrain.

The predictive equations of interpolation uncertainty presented in this research assume uniform uncertainty with distance to the nearest measurement, and it has been shown in this thesis that interpolation accuracy is highly non-stationary, as a result of variable terrain and thus variable spatial autocorrelation. The predictive equations, while simplistic and applicable to Kachemak Bay, are a good first step in estimating interpolation uncertainty for deterministic interpolation methods, despite their limitations. The predictive equations should be evaluated in other areas for validation, and to provide confidence in their estimates of uncertainty.

## LITERATURE CITED

- Aguilar, F.J., Agüera, F., Aguilar, M.A., Carvajal, F. (2005). Effects of terrain morphology, sampling density, and interpolation methods on grid DEM accuracy. *Photogrammetric Engineering and Remote Sensing*. 71, 805–816.
- Akkala A, Devabhaktuni VK, Kumar A. (2010). Interpolation techniques and associated software for Environmental Data. *Environmental Progress & Sustainable Energy*. 29(2): 134-41.
- Ali, T. A. (2004). On the selection of an interpolation method for creating a terrain model (TM) from LIDAR data. *Proceedings of the American Congress on Surveying and Mapping (ACSM) Conference 2004*, Nashville TN, U.S.A
- Anderson, E. S., Thompson, J. A. and Austin, R. E. (2005). LIDAR density and linear interpolator effects on elevation estimates, *International Journal of Remote Sensing*, 26: 18, 3889 — 3900
- Blaschke, T., Tiede, D. and Heurich, M. (2004). 3D landscape metrics to modeling forest structure and diversity based on laser scanning data. *International Archives of the Photogrammetry, Remote Sensing and Spatial Information Sciences* 36(8/W2), 129-132.
- Bloschl, G., Grayson, R. (2001). Spatial observations and interpolation. In: Grayson, R., Bloschl, G. (Eds.), *Spatial Patterns in Catchment Hydrology; Observations and Modelling*, Cambridge University Press, Cambridge, pp. 17–50.
- Bouma, A. H., Rapperport, M. L., Orlando, R C. & Hampton, M. A. (1980). Identification of Bedforms in Lower Cook Inlet, Alaska. *Sedimentary Geology*, 26, 157-177.
- Burrough, P.A. and McDonnell, R.A. (1998). *Principles of Geographical Information Systems*. Oxford, UK: Oxford University Press, 333p.
- Carlisle, B.H. (2005). Modelling the spatial distribution of DEM error. *Transactions in GIS* 9 (4), 521–540.
- Castiglioni, S., Castellarin, A., and Montanari, A. (2009). Prediction of low-flow indices in ungauged basin through physiographical space-based interpolation. *Journal of Hydrology*. 378, 272–280.
- Cebecauer, T., Hofierka, J., Suri, M. (2002). Processing digital terrain models by regularized spline with tension: tuning interpolation parameters for different input datasets. In: *Proceedings of Open Source Free Software GIS - GRASS Users Conference 2002*, Trento, Italy, 11-13 Sept. 2002.

- Chang, K. and Tsai, B. (1991). The effect of DEM resolution on slope and aspect mapping. *Cartography and Geographic Information Systems* 18, 69–77.
- Chaplot, V., Darboux, F., Bourennane, H., Legu dois, S., Silvera, N. and Phachomphon, K. (2006). Accuracy of interpolation techniques for the derivation of digital elevation models in relation to landform types and data density. *Geomorphology* 77(1-2), 126-141.
- Childs, Colin. (2004). “Interpolating Surfaces in ArcGIS Spatial Analyst.” *ArcUser*. Redlands, CA: ESRI Press.
- Declercq, FAN. (1996). Interpolation methods for scattered sample data: accuracy, spatial patterns, processing time. *Cartography and Geographical Information Systems* 23(3): 128–44.
- Desmet, PJJ. (1997). Effects of interpolation errors on the analysis of DEMs. *Earth Surface Processes and Landforms* 22: 563–580.
- Eakins, B. W. and L. A. Taylor. (2010). Seamlessly integrating bathymetric and topographic data to support tsunami modeling and forecasting efforts, in *Ocean Globe*, ed. by J. Bremen, ESRI Press, Redlands, 37–56.
- Erdogan, S. (2009). A comparison of interpolation methods for producing digital elevation models at the field scale. *Earth Surface Processes and Landforms*. 34, 366–376.
- Erdogan, S. (2010). Modelling the spatial distribution of DEM error with geographically weighted regression: An experimental study, *Computers and Geosciences*. 36, 34-43.
- ESRI. (2009). ESRI World 2D Imagery – ESRI ArcGIS Resource Centers, <http://resources.esri.com/arcgisonlineservices/>
- ESRI. (2010). ArcGIS Desktop Help 10.0 – How Spline works. ONLINE. Available: [http://help.arcgis.com/en/arcgisdesktop/10.0/help/index.html#/How\\_Spline\\_works/009z00000780000000/](http://help.arcgis.com/en/arcgisdesktop/10.0/help/index.html#/How_Spline_works/009z00000780000000/), 04/01/2012.
- Fisher, P. F. and Tate, N. J. (2006). Causes and consequences of error in digital elevation models. *Progress in Physical Geography* 30(4), 467-489.
- Friday, D.Z., L.A. Taylor, B.W. Eakins, K.S. Carignan, R. J. Caldwell, P.R. Grothe, and E. Lim. (2010). Digital Elevation Model of Kachemak Bay, Alaska: Procedures, Data Sources and Analysis.
- Galant, J.C and Wilson, J.P. (2000). Primary Topographic Attributes. In Wilson, J. and Gallant, J., editors, *Terrain analysis: principles and applications*. New York City NY: John Wiley and Sons, 51 – 85.

- Guo, Q., Li, W., Yu, H., Alvarez, O. (2010). Effects of topographic variability and lidar sampling density on several DEM interpolation methods. *Photogram. Eng. Remote Sensing*, 76, 1-12.
- Hare, R., Eakins, B., Amante, C. (2011). Modelling Bathymetric Uncertainty. *International Hydrographic Review*, 31 – 42.
- Horrillo, J., W. Knight, and Z. Kowalik. (2008). The Kuril Islands Tsunami of November 2006, Part II: Impact at Crescent City by local enhancement, *Journal of Geophysical Research*, 113.
- Isaaks, E. H. and Srivastava, R. M. (1989). An introduction to applied geostatistics. Oxford University press. New York, 561 p.
- Kowalik, Z., J. Horrillo, W. Knight, and T. Logan (2008). The Kuril Islands tsunami of November 2006. part I: Impact at Crescent City by distant scattering, *Journal of Geophysical Research*, 113.
- Li, J., and Heap, A.D. (2008). A review of spatial interpolation methods for environmental scientists. Geoscience Australia, Canberra.
- Liu, X., Zhang, Z., Peterson, J. and Chandra, S. (2007). LiDAR-derived high quality ground control information and DEM for image orthorectification. *GeoInformatica* 11(1), 37-53.
- Lloyd, C. D. and Atkinson, P. M. (2002). Deriving DSMs from LiDAR data with kriging, *International Journal of Remote Sensing*, 23: 12, 2519 –2524
- MacEachren, A.M., and J.V. Davidson, (1987). Sampling and isometric mapping of continuous geographic surfaces, *The American Cartographer*, 14(4):299–320.
- Mackaness, W. and Beard, M.K. (1993). Visualization of interpolation accuracy. *Proceedings Eleventh International Symposium on Computer-Assisted Cartography, Minneapolis, 1993 (AutoCarto 11)*: 228 – 37.
- Maune D. F., Kopp S.M., Crawford C.A. & Zervas C.E. (2007). Introduction, in *Digital Elevation Model Techniques and Applications: The DEM Users Manual*. 2nd Ed., ed. by D. F. Maune, American Society for Photogrammetry and Remote Sensing, Bethesda, 1–35.
- Meyers, D.E. (1994). Spatial Interpolation: An Overview. *Geoderma*, 62:17-28.
- Mitas, L. and Mitasova, H. (1999). Spatial interpolation. In Longley, P.A., Goodchild, M.F., Maguire, D.J. and Rhind, D.W., editors, *Geographical Information Systems, volume 1: principles and technical issues*, New York: Wiley, 481–92.

- Mitas, L., and H. Mitasova. (1988). General Variational Approach to the Interpolation Problem. *Computer and Mathematics with Applications*. Vol. 16. No. 12. pp. 983–992. Great Britain.
- Mitasova, H., and L. Mitas. (1993). Interpolation by regularized spline with tension, I, Theory and implementation, *Math. Geol.*, 25, 641–655.
- Mossa, J., and M.B. McLean. (1997). Channel plan-form and land cover changes on a mined river floodplain: Amite River, Louisiana, USA. *Applied Geography* 17:43-54.
- Peralvo, M., Maidment, D. (2004). Influence of DEM interpolation methods in drainage analysis. *GIS in Water Resources* CE 394K
- Podobnikar, T. (2005). Suitable DEM for required application. *Proceedings of the 4<sup>th</sup> International Symposium on Digital Earth*, Tokyo, Japan
- Robinson, TP, Metternicht GI. (2005). Comparing the performance of techniques to improve the quality of yield maps. *Agricultural System* 85: 19–41.
- Satake, K. (1988). Effects of bathymetry on tsunami propagation: Application of ray-tracing to tsunamis. *Pure Appl. Geophys.*, 126, 27-36.
- Smith S.L, Holland, DA, and Longley PA. (2005). Quantifying interpolation errors in urban airborne laser scanning models. *Geographical Analysis* 37(2): 200–224.
- Smith, S.L, Holland, D.A, and Longley, P.A. (2003). The effect of changing grid size in the creation of laser scanner digital surface models. *Geocomputation*.
- Smith, W. H. F., and D. T. Sandwell. (1997). Global sea floor topography from satellite altimetry and ship depth soundings. *Science* 277(5334), 1956-1962.
- Smith, W.H.F. (2004). Introduction to this special issue on bathymetry from space. *Oceanography*, 17(1), pp. 6–7.
- Soucy, M. and D. Laurendeau. (1996). Multiresolution surface modeling based on hierarchical triangulation, *Computer Vision and Image Understand.* 63, 1–14.
- Titov, V., González, F., Mofjeld, H., Venturato, A. (2003). *NOAA TIME Seattle Tsunami Mapping Project: Procedures, data sources, and products*. NOAA Tech. Memo. OAR PMEL-124
- Tobler, W. (1970). A computer movie simulating urban growth in the Detroit region. *Economic Geography*, 46(2): 234-240.
- U.S Department of Commerce, National Oceanic and Atmospheric Administration, National Ocean Service. (2008). Descriptive Report HI1983.

Vazquez RF, Feyen J. (2007). Assessment of the effects of DEM gridding on the predictions of basin runoff using MIKE SHE and a modelling resolution of 600 m. *Journal of Hydrology*. 334 (1-2): 73-87.